Cell Reports
Medicine

Article

Gut microbiome modified by bariatric surgery improves insulin sensitivity and correlates with increased brown fat activity and energy expenditure

Graphical abstract

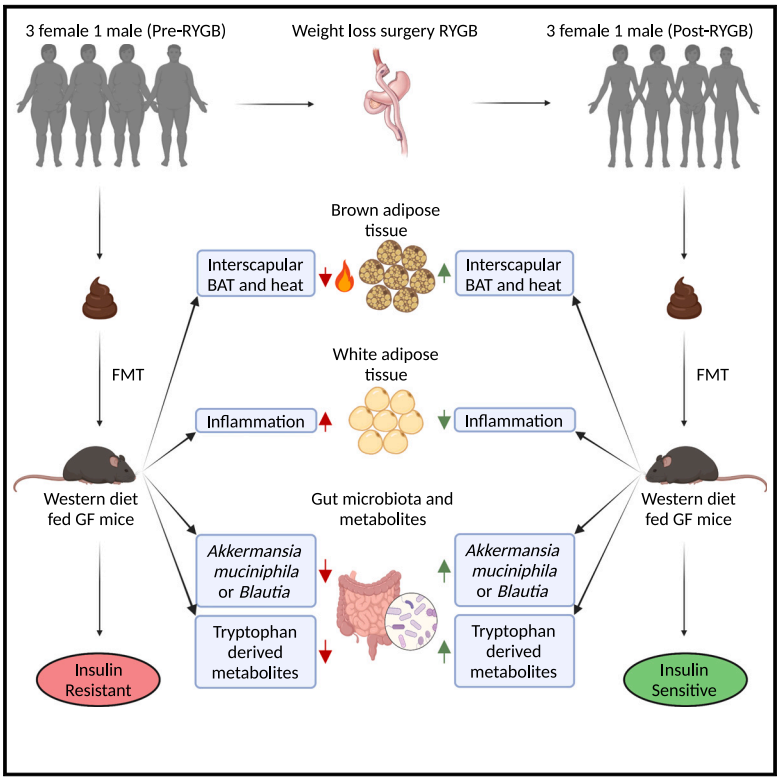

Highlights

- Post-RYGB FMT improves insulin sensitivity, energy expenditure, and brown adipose tissue
- Post-RYGB FMT mice exhibit reduced inflammation in white adipose tissue
- Mice harboring the post-RYGB FMT are enriched with beneficial microbes
- Increased tryptophan-derived metabolites, SCFAs, and acylcarnitines with post-RYGB FMT

Authors

Jitender Yadav, Tao Liang, Tairan Qin, ..., Johane P. Allard, Dana J. Philpott, Herbert Y. Gaisano

Correspondence

johane.allard@uhn.on.ca (J.P.A.), dana.philpott@utoronto.ca (D.J.P.), herbert.gaisano@utoronto.ca (H.Y.G.)

In brief

Yadav et al. apply a multiomics approach to study the effects of FMT from obese patients, pre- and post-RYGB surgery, into germ-free mice and show that the post-surgery stool improves host metabolism, with concomitant changes in microbiota composition and metabolomic differences compared with pre-surgery FMT mice.

Yadav et al., 2023, Cell Reports Medicine *4*, 101051
May 16, 2023
https://doi.org/10.1016/j.xcrm.2023.101051

CellPress

Cell Reports Medicine

CellPress
OPEN ACCESS

Article

Gut microbiome modified by bariatric surgery improves insulin sensitivity and correlates with increased brown fat activity and energy expenditure

Jitender Yadav,[1,17] Tao Liang,[2,3,17] Tairan Qin,[2,3,17] Nayanan Nathan,[1] Katherine J.P. Schwenger,[4] Lauren Pickel,[3,5] Li Xie,[2] Helena Lei,[7] Daniel A. Winer,[1,6,7,8] Heather Maughan,[9] Susan J. Robertson,[1] Minna Woo,[1,2,3,4,7] Wendy Lou,[10] Kate Banks,[11,16] Timothy Jackson,[12,13] Allan Okrainec,[12,13] Susy S. Hota,[3,14] Susan M. Poutanen,[6,15] Hoon-Ki Sung,[5,6] Johane P. Allard,[2,3,4,*] Dana J. Philpott,[1,6,18,*] and Herbert Y. Gaisano[2,3,*]

[1]Department of Immunology, University of Toronto, Toronto, ON, Canada
[2]Toronto General Hospital Research Institute, University Health Network, Toronto, ON, Canada
[3]Department of Medicine, University of Toronto, Toronto, ON, Canada
[4]Toronto General Hospital, University Health Network, Toronto, ON, Canada
[5]Translational Medicine Program, The Hospital for Sick Children, Toronto, ON, Canada
[6]Department of Laboratory Medicine and Pathobiology, University of Toronto, Toronto, ON, Canada
[7]Division of Cellular and Molecular Biology, Diabetes Research Group, Toronto General Hospital Research Institute, University Health Network, Toronto, ON, Canada
[8]Buck Institute for Research on Aging, Novato, CA, USA
[9]Ronin Institute, Montclair, NJ, USA
[10]Dalla Lana School of Public Health, University of Toronto, Toronto, ON, Canada
[11]Department of Comparative Medicine, University of Toronto, Toronto, ON, Canada
[12]Division of General Surgery, University of Toronto, Toronto, Canada
[13]Division of General Surgery, Toronto Western Hospital, University Health Network, Toronto, ON, Canada
[14]Infection Prevention and Control, University Health Network, Toronto, ON, Canada
[15]Department of Microbiology & Division of Infectious Diseases, University Health Network and Sinai Health, Toronto, ON, Canada
[16]Present address: Department of Pathology and Laboratory Medicine, Schulich Dentistry and Medicine, University of Western Ontario, London, ON, Canada
[17]These authors contributed equally
[18]Lead contact
*Correspondence: johane.allard@uhn.on.ca (J.P.A.), dana.philpott@utoronto.ca (D.J.P.), herbert.gaisano@utoronto.ca (H.Y.G.)
https://doi.org/10.1016/j.xcrm.2023.101051

SUMMARY

Alterations in the microbiome correlate with improved metabolism in patients following bariatric surgery. While fecal microbiota transplantation (FMT) from obese patients into germ-free (GF) mice has suggested a significant role of the gut microbiome in metabolic improvements following bariatric surgery, causality remains to be confirmed. Here, we perform paired FMT from the same obese patients (BMI > 40; four patients), pre- and 1 or 6 months post-Roux-en-Y gastric bypass (RYGB) surgery, into Western diet-fed GF mice. Mice colonized by FMT from patients' post-surgery stool exhibit significant changes in microbiota composition and metabolomic profiles and, most importantly, improved insulin sensitivity compared with pre-RYGB FMT mice. Mechanistically, mice harboring the post-RYGB microbiome show increased brown fat mass and activity and exhibit increased energy expenditure. Moreover, improvements in immune homeostasis within the white adipose tissue are also observed. Altogether, these findings point to a direct role for the gut microbiome in mediating improved metabolic health post-RYGB surgery.

INTRODUCTION

Obesity, metabolic syndrome, and type 2 diabetes (T2D) have reached alarming epidemic levels globally. Obesity is a multifactorial and complex disease, influenced by host biology, genetics, and environmental factors. For the most severe cases of obesity (body mass index [BMI] > 40 or >35 with associated co-morbidities), bariatric surgery, specifically, the Roux-en-Y gastric bypass (RYGB), is still the mainstay treatment to induce durable improvement.[1,2] Bariatric surgery achieves both rapid and sustained weight loss and can reduce the requirement for medications used for T2D and metabolic syndrome.[1–3] However, the underlying mechanism for reversing insulin resistance remains elusive. While the beneficial effects of bariatric surgery were first attributed to the greatly reduced size of the stomach and intestinal absorptive surface exposure for nutrients, it was later found that the altered surgical intestinal anatomy brought about additional changes that contributed to the improvement

in metabolism and weight loss. These changes include the exaggerated release of glucagon-like peptide-1 (GLP-1) and peptide YY (PYY) from intestinal L cells,[4,5] both acting synergistically on pancreatic islets to restore glucose-stimulated insulin secretion[4,6,7] and on brain centers to improve sensitivity to satiety hormones to reduce food intake,[8,9] as well as alterations in nutrient sensing[10] and bile acid metabolism.[11] Bariatric surgery also changes the expression profile of miRNAs in pancreatic islets and improves glucose-mediated insulin secretion.[7] Notably, bariatric surgery profoundly changes the composition and functional output of the gut microbiota,[12,13] which are thought to mediate certain metabolic improvements in patients post-surgery.

The gut microbiota can influence the efficiency of energy harvest from ingested nutrients and fat storage by the host, which are both upregulated by the gut microbiota of obese subjects.[14–16] These characteristics of the gut microbiota can be transferred to recipient humans or mice by fecal microbiota transplantation (FMT), inducing reversible transmission of the obesity phenotype.[14–19] Interestingly, FMT from mice subjected to RYGB into germ-free (GF) recipient mice show that the RYGB-associated microbiota independently triggers a decrease in the recipients' weight as well as their adiposity.[20] In studies of human FMT into GF mice, the post-RYGB surgery stool from obese subjects was also shown to promote a reduction in fat deposition[21] and improvement in blood glucose control and diabetes resolution in recipient animals.[22,23] While these important studies support a link between gut microbiota changes and an improvement in certain aspects of host physiology following bariatric surgery, the well-known heterogeneity of obesity-associated metabolic parameters, compounded by the even more complex heterogeneity of the gut microbiota, has limited the ability to formulate causal inferences and restricted any mechanistic understanding of how the gut microbiota promotes these changes.

Here, we circumvent inherent limitations of previous experimental strategies by performing paired FMT from the same obese patient (BMI > 40) pre- and post-RYGB surgery into GF mice, thereby eliminating potential interindividual variation. Moreover, we challenged pre- and post-surgery colonized mice to an established preclinical obesity/T2D model by feeding animals a Western-style diet (WD). As expected, RYGB surgery altered the composition of the gut microbiota in patients as well as in colonized mice receiving these stools compared with animals harboring pre-surgery microbiota. Concomitant changes in metabolites were also observed. Strikingly, we found that FMTs from the same patient pre- and post-surgery conferred the transfer of insulin-resistant and insulin-sensitive phenotypes, respectively, and that the improved glucose homeostasis mediated by the post-surgery FMT was associated with increased brown fat mass and activity, increased energy expenditure, and a reduced inflammatory environment within the visceral white adipose tissue. Taken together, these findings demonstrate a direct role of the gut microbiota in modulating metabolic parameters post-RYGB surgery and give support to the use of prebiotics or probiotics, as well as healthy human FMT applications, to improve metabolism in obese individuals, with the ultimate goal of avoiding the need for surgery.

RESULTS

RYGB surgery results in improved clinical parameters in obese patients

We aimed to test the effects of RYGB surgery on the gut microbiota and whether alterations in the gut microbiota of patients after bariatric surgery were an important factor in metabolic improvement. Four morbidly obese individuals who had a mean age of 47 years (SD ± 13) and a BMI of 45.1 kg/m^2 (SD ± 3.9) were selected, and three of the four patients were female. According to Diabetes Canada guidelines, three of the four patients had a prediabetic or diabetic status; further clinical data can be found in Table 1. Fecal samples were collected prior to bariatric surgery and at 1 (patients T12, T73, and T79) or 6 (patient T41) months post-RYGB (see Figure 1A). Overall, BMI significantly decreased post-RYGB in all four participants, and fasting glucose as well as homeostatic model of assessment of insulin resistance (HOMA-IR) also significantly decreased. There were no significant improvements in HbA1c in those whose samples were collected at 1 month post-RYGB. However, in the individual from whom the sample was collected at 6 months post-RYGB, HbA1c did significantly improve (Table 1). This is likely because HbA1c reflects average blood glucose levels of 2–3 months[24] and therefore the impact of bariatric surgery is not seen at 1 -month post-RYGB. In addition, these four individuals were representative of the range of metabolic derangements in the general bariatric population with regard to clinical and biochemical parameters (Table S1).[25,26]

WD-fed mice colonized with patients' post-RYGB fecal samples show restored metabolic health compared with mice receiving pre-surgery samples

We next asked whether the improvements in metabolic health of these patients following RYGB surgery could be mediated to some degree by surgery-induced alterations in the composition of the gut microbiota. To test this, we employed GF mice colonized with fecal samples from patients, since this approach is most commonly used for establishing a causal role of microbiome alterations in human disease. Fecal samples from the same patient pre- (and prior to commencing a low-calorie diet) and post-surgery were gavaged into cohorts of GF mice. We then tested whether alterations in the gut microbiota after surgery could improve metabolic outcomes compared with those mice receiving the paired samples prior to surgery (Figure 1A). GF mice were first "primed" on a WD (34% sucrose and 22% fat by weight) for 10 weeks and then maintained on this diet for an additional 12 weeks after the FMT (Figure 1B). While there was a trend of post-surgery FMT mice exhibiting less body weight compared with pre-surgery FMT mice, overall, there were no significant differences in body weight between the two groups (Figure S1A). The different organ weights also did not differ between the mouse groups (Figure S1A).

Next, we performed intraperitoneal insulin tolerance tests (ITTs) and intraperitoneal glucose tolerance tests (IPGTTs) to evaluate whole-body insulin sensitivity comparing the two mouse groups. In the ITT, the blood glucose levels for patient T41 were significantly lower in the post-RYGB FMT mice

Table 1. Patients' clinical parameters before and after bariatric surgery

	Patient donor			
Parameter	T12	T41	T73	T79
Age (years)	27	56	54	51
Gender	female	male	female	female
Baseline				
Weight (kg)	152.41	123.6	118.2	115
BMI (kg/m^2)	50.34	42.77	45.60	41.63
T2D diagnosis[a]	prediabetes	T2D	T2D	no
T2D medications	none	insulin 40 U/day, gliclazide 60 mg/day, Janumet[b] 2×/day	none	none
HbA1c	0.060	0.071	0.065	0.055
Fasting glucose (mmol/L)	4.8	9.7	7.0	5.7
HOMA-IR[c]	N/A	15.3	8.8	6.4
1 or 6 months post-RYGB				
Fecal sample post-RYGB (used for FMT)	1 month	6 months	1 month	1 month
BMI (kg/m^2)	43.9	31.8	39.79	37.45
HbA1c	0.060	0.054	0.065	0.053
Fasting glucose (mmol/L)	4.4	4.5	5.8	4.8
HOMA-IR	3.7	4.9	2.8	1.7
T2D medications	none	insulin 10 U/day	none	none

BMI, body mass index; HbA1c, hemoglobin A1c; HOMA-IR, homeostatic model of assessment of insulin resistance; T2D, type 2 diabetes; N/A, samples at this time point were not taken.
[a]Diabetes Canada definitions for diabetes, fasting blood glucose ≥ 7 mmol/L, HbA1c ≥6.5%; and prediabetes, fasting blood glucose 6.1–6.9 mmol/L, HbA1c 6.0%–6.4%.
[b]Janumet (50 mg sitaglyptin/1,000 mg metformin).
[c]HOMA-IR: <1.0 is insulin sensitive, >1.9 is early insulin resistance, >2.9 is significant insulin resistance.

compared with pre-RYGB FMT mice after intraperitoneal insulin injection (Figure 1C), which was also similar for the other three patients (Figure S1B). Area under the curve (AUC) in the post-RYGB FMT mice for all four of the patients was significantly lower than in the pre-RYGB FMT group (Figures 1D and S1C). With the IPGTT tests, WD-fed post-RYGB FMT mice for patient T41 showed a significant improvement in glucose tolerance compared with mice with pre-surgery FMT after glucose injection (Figure 1E), which again was more or less similar to that observed for mice receiving post-surgery FMT from the three other patients (Figure S1D). Also similar to what we observed during the ITT test, the AUC was lower in post-RYGB FMT mice with each patient sample compared with pre-RYGB FMT mice (Figures 1F and S1E). Notably, pre-RYGB FMT mice displayed higher levels of insulin than post-RYGB FMT mice (Figures 1G, 1H, S1F, and S1G), indicating that mice receiving the pre-RYGB stool were hyperinsulinemic, reflecting an insulin-resistant state.[27] We then explored whether the increased insulin levels in pre-RYGB FMT mice were due to an increase in β cell mass or increased secretory capacity of each β cell. Between the pre- and post-RYGB FMT mice, we saw no significant changes in islet number/pancreatic area, β cell area/pancreatic area, or HOMA-β cell (Figures S1H–S1K). This suggests that the reduced blood insulin levels post-RYGB were likely attributed to the overall improvement in insulin sensitivity that resulted in a reduction in insulin secretory demand. Overall, these data suggest that the post-RYGB microbiota was able to restore normal glucose regulation and insulin sensitivity in the WD-fed mice, despite not altering body weight compared with that of pre-RYGB FMT WD-fed mice.

Post-RYGB FMT increased energy expenditure and was associated with an increase in brown adipose tissue mass and activity in WD-fed mice

We next determined if the enhanced insulin sensitivity in post-RYGB FMT mice could be attributed to an increase in energy expenditure as a potential mechanism. Accordingly, mice were analyzed using metabolic cages to quantify energy expenditure, which include the following parameters: oxygen consumption (VO_2), respiratory exchange ratio (RER), and heat production. As shown in Figures 2A and 2B, the post-RYGB FMT mice had improved energy expenditure compared with the pre-RYGB FMT mice, as reflected by higher oxygen consumption and increased heat production. With the mouse cohorts representing individual patients, there was a trend for the volume of oxygen consumption and heat production to be higher in post-RYGB mice (Figures S2A and S2B). The RER of the combined post-RYGB FMT mice was significantly higher than in the pre-RYGB FMT mice (Figure 2C), a trend also observed in mouse cohorts representing individual patients (Figure S2C), suggesting that these animals were better at metabolizing sugars/carbohydrates and possibly micronutrients than the pre-RYGB FMT mice. Food and water intake did not differ between the two groups (Figures S2D and S2E).

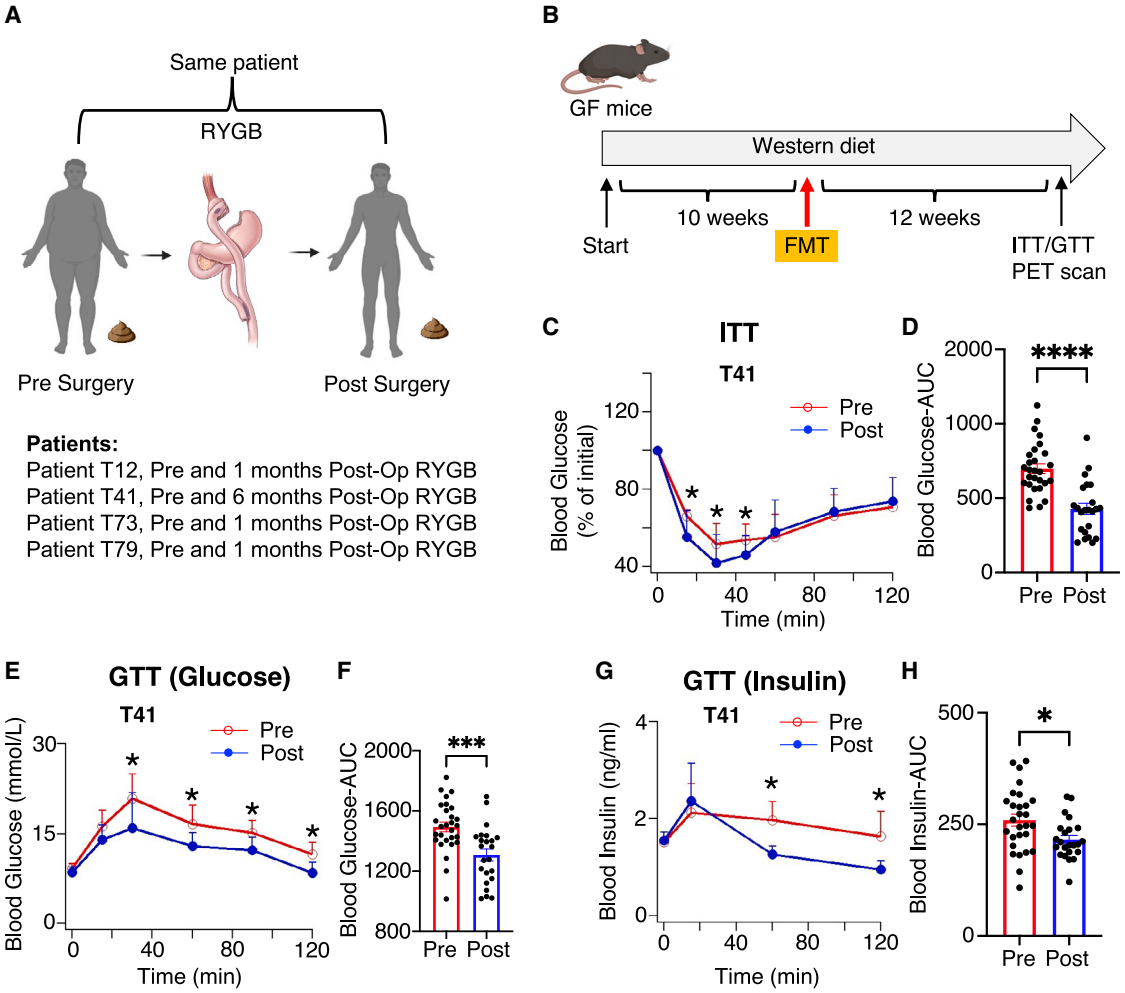

Figure 1. Improved metabolic outcomes in mice receiving stool samples from patients post-RYGB surgery

(A) Fecal samples were collected from four morbidly obese human patients before and 1 or 6 months after RYGB surgery.

(B) Experimental design: germ-free (GF) mice were maintained on a Western diet (WD; 21% fat and 34% sucrose by weight) for 10 weeks, transplanted with pre- or post-RYGB surgery fecal samples from four obese patients (T12, T41, T73, and T79), and maintained on the WD for 12 subsequent weeks in the GF facility. Metabolic testing was then performed, followed by sacrifice and tissue collection.

(C) Representative intraperitoneal insulin tolerance test (ITT) kinetic plot. ITT was performed on WD-fed pre- and post-RYGB FMT mice (from patient T41) at week 13 (after FMT). Mice were fasted for 4 h and then injected intraperitoneally with insulin (1.5 IU/kg body weight) (pre n = 8, post n = 5). Blood samples were taken from the tail vein of the same animals at the times indicated, and blood glucose concentration was determined as indicated in STAR methods.

(D) Combined area under the curve (AUC) of blood glucose levels from ITT. AUC was calculated for mouse cohorts of the individual patients and then combined to show values for the mouse cohorts for all four patients. Each dot represents one mouse/biological replicate (pre n = 28, post n = 23).

(E) Representative intraperitoneal glucose tolerance test (IPGTT) kinetic plot. IPGTT test was performed in WD-fed mice colonized with pre- or post-RYGB microbiota from patient T41 at week 14 (after FMT). Mice were fasted for 16 h, and glucose (1.5 mg/g body weight) was then administered intraperitonially. Blood glucose levels were measured at the indicated time points after glucose injection (pre n = 8, post n = 5).

(F) Combined AUC for blood glucose from IPGTT. AUC was calculated for the individual mouse cohorts representing one patient and combined to show values for the mouse cohorts of all the four patients. Each dot represents one mouse/biological replicate (pre n = 28, post n = 23).

(G) Blood samples were collected at 0, 15, 60, and 120 min during IPGTTs, and serum insulin levels were measured by ELISA (pre n = 8, post n = 5).

(H) AUC from insulin values from IPGTT. Each dot represents one mouse/biological replicate (pre n = 28, post n = 23). Data displayed as mean ± SEM. Statistical significance was calculated using two-tailed unpaired t test; *p < 0.05, ***p < 0.0005, ****p < 0.0001.

A major contribution to the increase in energy expenditure is non-shivering thermogenesis generated by brown adipose tissue (BAT),[28] which we therefore assessed next. To measure BAT thermogenic activity, we measured the uptake of [^{18}F]fluorodeoxy-D-glucose (FDG) into the BAT after acute cold exposure (see STAR Methods), detected by positron emission tomography (PET). Co-registration of the PET images with the computed tomography (CT) images allowed a comparison of the volume of [^{18}F]-FDG uptake versus the total body mass.[29] Notably, mice colonized with the post-RYGB microbiota following 14 weeks of WD had a much higher [^{18}F]-FDG uptake into the BAT than the mice receiving the pre-RYGB FMT (Figures 2D, 2E, S2F,

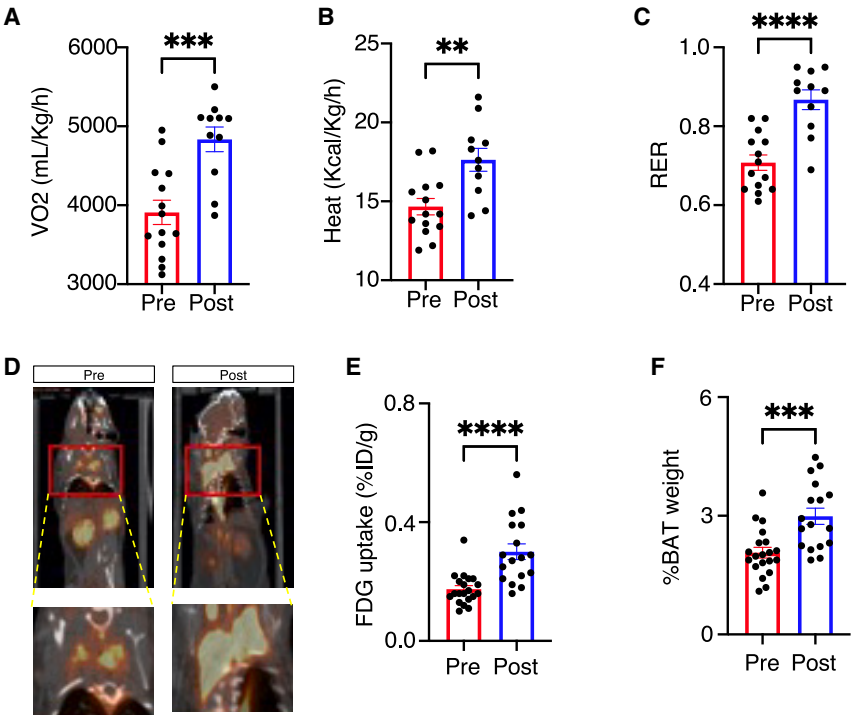

Figure 2. Post-RYGB microbiota increased heat production and interscapular brown adipose tissue in Western-diet-fed mice

Metabolic cage studies were performed in pre- and post-RYGB FMT mouse groups in CLAMP metabolic cages at week 15 after FMT. Mice were housed in the metabolic cage chambers for 48 h, with the first 24 h being to familiarize the animals to their new environment. Data shown are from the second 24-h period.

(A) Oxygen consumption normalized to body weight. Each dot represents one mouse/biological replicate (pre n = 14, post n = 11).

(B) Heat (energy expenditure) normalized to body weight. Each dot represents one mouse/biological replicate (pre n = 14, post n = 11).

(C) Respiratory exchange ratio (RER) was calculated as the ratio of carbon dioxide production volume to oxygen consumption volume. Each dot represents one mouse/biological replicate (pre n = 14, post n = 11).

(D) Micro-PET/CT imaging of BAT in mice after overnight (14–16 h) cold treatment (4°C). A view of the fused PET/CT image using [^{18}F]FDG ([^{18}F]-fluorodeoxy-D-glucose) is shown for pre- and post-RYGB FMT mice. The area in the red box corresponds to interscapular brown adipose tissue. Note the large increase in [^{18}F]-FDG accumulation in the BAT.

(E) Quantitative analysis of [^{18}F]FDG uptake in the BAT. Values of percentage injected dose per gram of tissue (%ID/g) are presented. Each dot represents one mouse/biological replicate (pre n = 20, post n = 17).

(F) Weight of isolated interscapular BAT from pre- and post-RYGB FMT mice Each dot represents one mouse/biological replicate (pre n = 20, post n = 17). Data displayed as mean ± SEM. Statistical significance was calculated using two-tailed unpaired t test; **p < 0.005, ***p < 0.0005, ****p < 0.0001.

and S2G), thus providing visual evidence of increased thermogenesis of BAT in the post-RYGB FMT mice. Along with its increased activity, the interscapular BAT weight was also significantly increased in post-RYGB FMT mice compared with pre-RYGB FMT mice (Figures 2F and S2H), likely contributing to the increased energy expenditure in post-RYGB FMT mice.

We then further assessed the interscapular BAT to explain the BAT activity. Brown adipocytes are characterized by the presence of multiple lipid droplets and numerous mitochondria that abundantly express uncoupling protein 1 (UCP1), an essential protein for thermogenesis.[28,30] These lipid droplets shrink, and UCP1 is upregulated as BAT activity increases. Since the post-RYGB FMT in WD-fed mice significantly improved insulin sensitivity (Figure 1) and increased energy expenditure compared with mice receiving the pre-RYGB FMT (Figure 2B), we next investigated the role of the microbiota in altering BAT morphology as well as its activity at the tissue level. We first compared the size of lipid droplets in BAT and found that BAT from post-RYGB FMT mice contained smaller lipid droplets than pre-RYGB BAT (Figures 3A, 3B, and S3A). We next performed immunohistochemical staining for UCP1 expression in BAT and noted that the area of UCP1 staining was higher in the post-RYGB FMT mice compared with the pre-RYGB FMT mice (Figures 3C, 3D, and S3B). These findings are in line with the idea that higher expression of UCP1 in the BAT of WD-fed mice receiving the post-RYGB microbiota may be contributing to the increased energy expenditure and insulin sensitivity in these animals. Collectively, these data indicate that the effects of post-RYGB microbiota on BAT mass and activity can contribute to an improvement in metabolic health even under conditions of continued WD feeding.

Visceral adipose tissue from mice colonized with post-RYGB FMT exhibited reduced inflammation

Visceral adipose tissue (VAT), particularly when inflamed, can promote the development of systemic insulin resistance.[31,32] We therefore analyzed the effects of pre- or post-RYGB FMT on VAT inflammation in WD-fed mice. VAT mass and size of adipocytes were not different between the two groups of mice (Figures S3C and S3D). Nevertheless, gene expression analysis of markers that reflect inflammatory and regulatory environments within adipose tissue[33] showed that VAT from the post-RYGB FMT mice had a reduced inflammatory signature, with decreased expression of *Tnf-α*, *Ccl2* (also known as monocyte chemoattractant protein 1, *MCP-1*), and *Elane* (neutrophil elastase), compared with those mice receiving the pre-RYGB microbiota (Figure 3E). Reduced expression of *Tnf-α* and *Elane* was also observed in the subcutaneous adipose tissue (SAT) in the post-RYGB mice (Figure S3E). We did not observe any differences in *Adgre1*, *Il1b*, *Nos*, or *Il10* expression in the VAT between the two groups (Figures S3G and S3H).

Also key in controlling obesity-related inflammation, as well as the energy status of the host, Sirtuin-1 (encoded by *Sirt1*) can diminish inflammation by suppressing NF-κB activation,[34] and it has been shown to protect against diet-induced metabolic dysfunction in adipocytes.[35,36] Consequently, we examined the

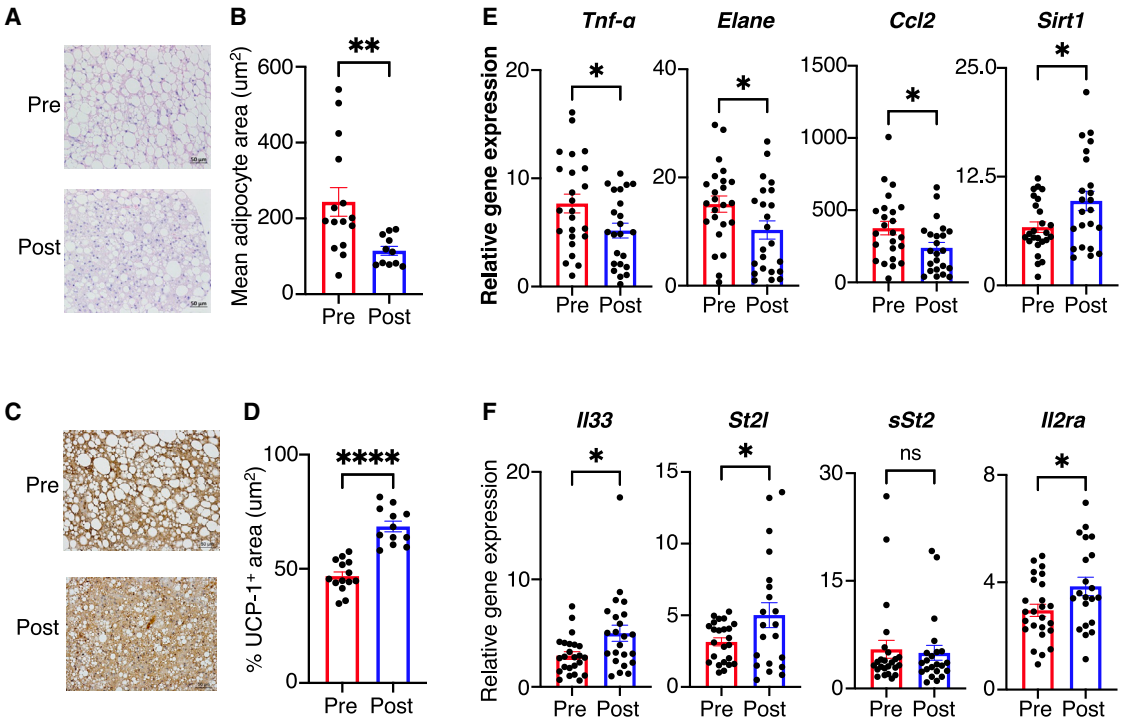

Figure 3. Microbiota from patients post-RYGB transplanted into mice leads to improvement in brown adipose tissue (BAT) and visceral adipose tissue (VAT) health

(A) Representative hematoxylin and eosin-stained sections of BAT of mice receiving fecal microbiota transplanted from patients pre- and post-RYGB. Scale bars, 50 μm.

(B) Frequency distribution of the surface area of the lipid droplets in BAT from (A). Each dot represents one mouse/biological replicate (pre n = 15, post n = 11).

(C) Representative immunohistochemical images for uncoupling protein 1 (UCP1; brown stain) in BAT of mice receiving pre- and post-RYGB FMT from individual patients. Scale bars, 50 μm.

(D) CellProfiler was used to quantify relative UCP1-positive area in BAT of pre- and post-RYGB FMT mice. Data are represented as UCP1-positive area relative to UCP1 area plus lipid droplet area in order to exclude background and other inconsistent tissue features. Each dot represents one mouse/biological replicate (pre n = 14, post n = 12).

(E) The relative expression levels of inflammatory genes and *Sirt1* in VAT of mice receiving pre- and post-RYGB microbiota from individual patients measured by qRT-PCR.

(F) Expression of T regulatory (Treg) and Th2-associated markers was analyzed in VAT of mice receiving pre- and post-RYGB microbiota of individual patients measured by qRT-PCR. Each dot represents one mouse/biological replicate (pre n = 24–25, post n = 21–23). Data displayed as mean ± SEM. Statistical significance was calculated using two-tailed unpaired t test; *p < 0.05, **p < 0.005, ****p < 0.0001; ns, not significant.

expression of the *Sirt1* gene by qPCR in VAT and SAT. Interestingly, and compared with pre-RYGB FMT mice, we detected a significant upregulation of *Sirt1* mRNA expression in VAT as well as SAT of post-RYGB FMT mice compared with pre-RYGB FMT mice (Figures 3E and S3E). Taken together, reduced inflammatory signaling and upregulation of Sirtuin-1 expression in the white adipose tissue may contribute to the systemic increase in insulin sensitivity that we see in these animals.

Since inflammation in adipose tissue is accompanied by a reduction in resident regulatory T cells (Tregs) and group 2 innate lymphoid cells (ILC2s), which can contribute to obesity-associated adipose dysfunction and insulin resistance,[37] we further looked at the expression of genes important in these pathways. We found that expression of *Il33* and *St2l* (the receptor for IL-33) was higher in the VAT of WD-fed mice colonized with the post-RYGB microbiota compared with the pre-RYGB FMT mice (Figure 3F), suggesting a possible effect on numbers and functionality of ILC2s.[38] Expression of *Il2ra*, which is regulated by IL-33 and highly expressed by Tregs,[39,40] was also increased in the VAT of mice harboring the post-RYGB microbiota (Figure 3F). These observations are consistent with the reduced inflammatory cytokine environment (Figure 3E). On the other hand, the expression of *sSt2*, which is the decoy receptor of IL-33 and attenuates its signaling, was not different between pre- and post-RYGB FMT mice (Figure 3F). Expression of the cytokines IL-5 and IL-13 was not detected (data not shown). No difference in expression of these markers between pre- and post-RYGB FMT mice was observed in the SAT (Figure S3F). We also did not observe any difference in the expression of beiging markers (*Ucp1*, *Cox8b*, and *Pat2*) in the VAT between the two groups (Figure S3I), which may be explained by the fact that we did not expose the animals to cold prior to euthanasia, and beiging marker expression is induced upon these conditions.[41] Taken together, these findings indicate that VAT from post-RYGB FMT mice is in a reduced inflammatory state compared with mice colonized with the pre-RYGB microbiota, and the

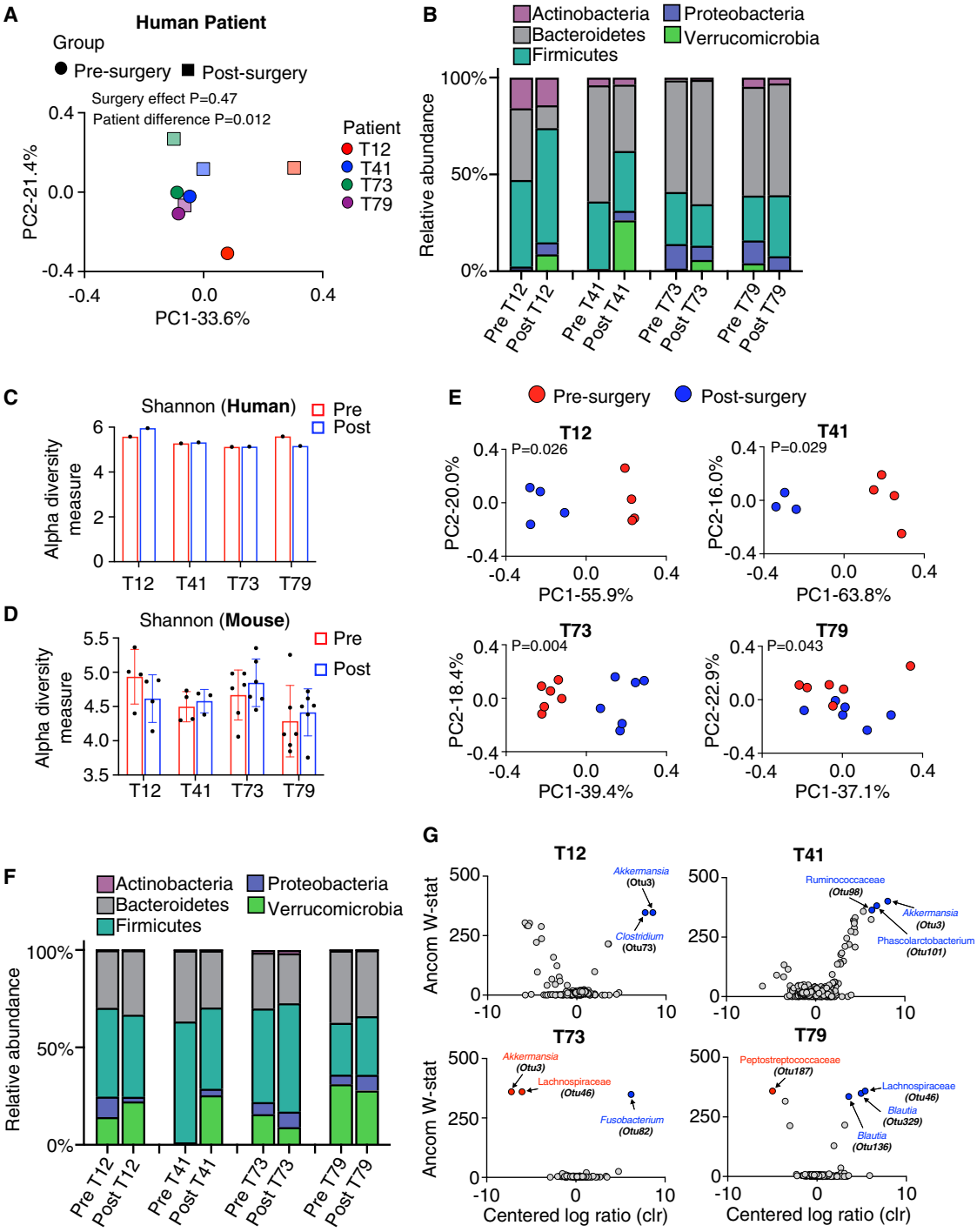

Figure 4. Alterations in the composition of the intestinal microbiota are observed in mice receiving fecal microbiota transplants (FMTs) from pre- and post-RYGB stool obtained from four obese patients

(A) Bray-Curtis PCoA plot shows change in community structure of pre- and post-RYGB surgery in each patient. Each dot or square represents one biological replicate (pre n = 4, post n = 4).

(B) Relative abundances of bacteria phyla in pre- and at 1 or 6 months post-RYGB surgery for the four human patient fecal samples (pre n = 4, post n = 4).

(C) Alpha diversity measurement (Shannon index) of the microbiota from fecal samples pre- and post-RYGB surgery in each patient (pre n = 4, post n = 4).

(D) Alpha diversity (Shannon index) between pre- and post-RYGB FMT microbiota in mice for each patient. Each dot represents one mouse/biological replicate (pre n = 4–6, post n = 3–6 per patient). Data displayed as mean ± SEM.

(legend continued on next page)

enhanced expression of regulatory pathway components may reflect better local homeostasis within the tissue.

Changes in microbiota composition observed in obese patients post-RYGB surgery are partially reflected in mice colonized with the post-RYGB stool

To determine if bacterial composition of the microbiota was altered in patients post-RYGB surgery and to examine if there were common signatures in mouse cohorts colonized with these fecal samples, DNA was extracted, and compositional analysis was done by sequencing of the 16S rRNA gene. Sequences per sample ranged from 22,666 to 137,137, and the average number of sequences per sample was 42,817 (Figure S4A). While we had only one stool sample from each patient pre- and post-surgery and are therefore limited in our interpretations, we did observe changes in microbiome composition after RYGB surgery (Figure 4A). Examining the relative abundances of phyla between pre- and post-surgery stool suggested that there was an increase in Verrucomicrobia in T12, T41, and T73 (Figure 4B). Very little change was observed in the alpha diversity in any of the patients after RYGB surgery (Figure 4C).

For mice colonized with the patient fecal samples, fecal DNA was extracted at 12 weeks after FMT, and gut microbial composition was assessed by 16S rRNA sequencing. The alpha diversity of pre- compared with post-RYGB-colonized mice was not different (Figure 4D). Permutational analysis of variance (PERMANOVA) of the principal coordinates analysis (PCoA) plots generated from Bray-Curtis distance matrices demonstrated that the pre- and post-RYGB FMT mice had significantly distinct microbiotas in the fecal pellet ($p < 0.05$; Figure 4E). Relative abundance plots showed distinctive community structure associated with the pre- versus post-RYGB fecal pellets, which were dominated by Verrucomicrobia in post-RYGB samples from mice colonized with stool from patients T12 and T41 (Figures 4F and 4G). In mice receiving FMT from patient T79 post-RYGB, there was an increase in abundance of *Blautia* (Figure 4G). The differences in beta diversity and differential abundances of taxa (Ancom analysis) were not seen with the pooled data from all the pre- and post-RYGB mice and human patients (Figures S4B and data not shown). The PCoA plots generated by combining individual patients with respective mice cohorts suggested that the difference between pre- and post-RYGB microbiota was significantly different with the T12, T41, and T73 cohorts, and it was not significantly different with T79 (Figure S4C). This observation is likely linked to the fact that this patient's post-surgery microbiota was similar to the pre-surgery microbiota (Figures 4A and S4C). Bray-Curtis distance plots suggest that the related pre- or post-RYGB mouse pairs were more similar to each other than the non-related pre- or post-RYGB mouse sample pairs (Figures S4D and S4E). We also observed from the Bray-Curtis distance plots that the related patient-mice pairs were more similar to each other than the non-related patient-mice sample pairs (data not shown). The targeted relative abundances of bacterial taxa were also quantified by qPCR. These data supported the 16S rRNA sequencing that suggested an increase in relative abundance of *Akkermansia muciniphila* in post-RYGB fecal samples from mice colonized with stool from patients T12 and T41 (Figure S4F). *Blautia* spp. abundances were significantly higher in post-RYGB fecal samples from mice colonized with stool from patients T73 and T79 (Figure S4G). Abundances of other taxa, including members of the Ruminococcaceae and Lachnospiraceae families, did not differ in their relative abundances in mice colonized by pre- or post-RYGB microbiota (Figures S4H and S4I).

Next, we looked at the metabolite composition in stool samples of pre- and post-RYGB mice. Volcano plots suggest that there were differences between the pre- and the post-RYGB metabolites in all patient cohorts (Figure 5A). We observed that the short-chain fatty acids (butyric acid), tryptophan metabolites (tryptamine, indole propionic acid, serotonin), and acylcarnitine (C5:1, C16:1-OH) were higher in post-RYGB fecal samples from mice colonized with stool samples from patients T12 and T41 (Figure 5A). In the mice colonized with patient T73 stool samples, the level of valeric acid (a short-chain fatty acid) was higher in post-RYGB mice. In T79 patient stool sample-colonized mice, the acylcarnitine levels were higher, and various amino acids (e.g., tyrosine and glycine as well as the branched-chain amino acids, valine, leucine, and isoleucine) were lower, in post-RYGB mice compared with pre-RYGB mice (Figure 5A). Interestingly, in the heatmap (from all patient cohorts), we observed that there were many differences in metabolites between the pre- and the post-RYGB mouse fecal samples (Figures 5B and S5A). Principal-component analysis (PCA) plots of pooled mouse samples from all the patient cohorts suggest that there was a significant difference in the metabolites between pre- and post-RYGB mice (Figure S5A). We then looked at the individual metabolites in the pooled samples and observed that the levels of lactic acid, pyruvic acid, and various amino acids (e.g., ornithine, arginine, glycine, and tyrosine) were significantly decreased in post-RYGB mouse stool samples compared with pre-RYGB mice (Figures 5B and 5C). Moreover, the tryptophan metabolites (tryptamine, indole acetic acid, indole propionic acid, and serotonin) and acylcarnitines (e.g., long-chain acylcarnitines, C12, C14, C16, and C18) were significantly higher in post-RYGB mouse stool samples compared with the pre-RYGB mice (Figures 5B, 5D, and 5F). For the short-chain fatty acids, valeric acid levels were significantly higher in post-RYGB mice, whereas propionic acid and isobutyric acid were trending higher (Figures 5B and 5E). We did observe more or less similar trends with the human stool metabolites as well

(E) Bray-Curtis PCoA plots show significant difference in the microbiota from the pre- (red dots) and post-RYGB FMT (blue dots) of mice 12 weeks after microbiota transfer from the four individual patients. Each dot represents one mouse/biological replicate (pre n = 4–6, post n = 3–6 per patient). PERMANOVA $p < 0.05$ (p value corrected by the Benjamini-Hochberg method).

(F) Relative abundances of bacterial phyla in pre- and post-RYGB FMT mice from each patient (pre n = 4–6, post n = 3–6 per patient).

(G) The analysis of composition of microbiomes (ANCOM) volcano plots for pre- and post-RYGB FMT mice from each patient. The W value represents the number of times the null hypothesis was rejected for a given species. The bacterial taxa significantly different abundances are labeled and colored blue (increased in post-RYGB FMT mice) or red (decreased in post-RYGB FMT mice) (pre n = 4–6, post n = 3–6 per patient).

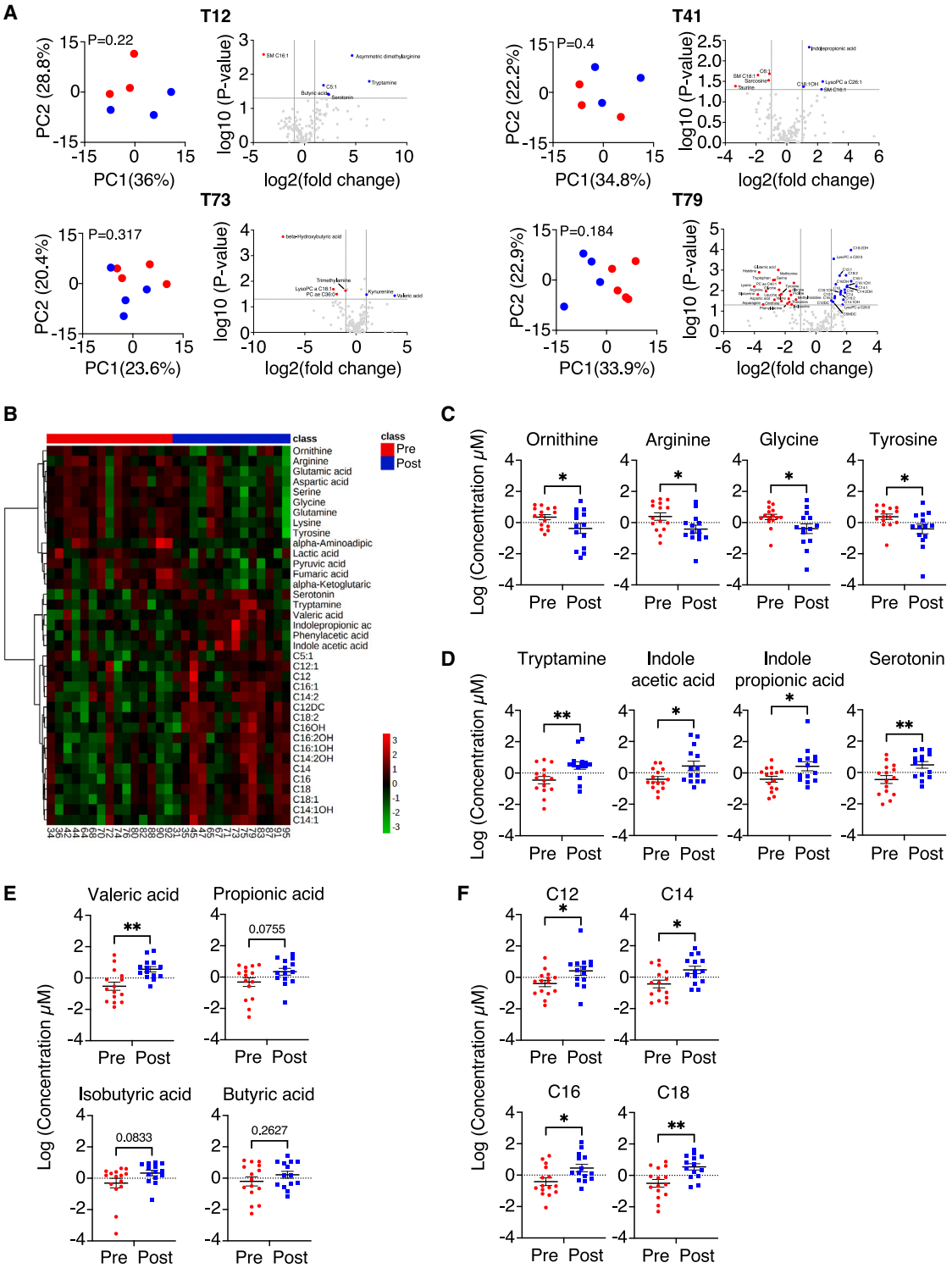

Figure 5. Comparison of fecal metabolite composition in pre- and post-RYGB FMT mice

(A) PCA and volcano plots for fecal metabolites from the pre- and post-RYGB FMT mice (pre, red dots; post, blue dots). Each dot represents one mouse/biological replicate (pre n = 3–4, post n = 3–5 per patient).

(legend continued on next page)

(Figures S5B, S5C, S5D, S5E, and S5F). The PCA plots for pooled patient samples showed a significant difference in metabolites between pre- and post-RYGB (Figure S5B). Taken together, increases in tryptophan metabolites, short-chain fatty acids, and acylcarnitines and decreases in amino acids (e.g., ornithine, arginine, glycine, and tyrosine), organic acid, and lactic acid were observed in the fecal samples of mice colonized with post-RYGB microbiota, correlating with improvements in overall metabolic health.

DISCUSSION

Bariatric surgery, in particular RYGB, is effective in reversing insulin resistance,[42] although the underlying mechanisms are still not fully understood. Findings from previous work in mouse models of RYGB suggest that the metabolic improvements may be causally related to changes in the gut microbiome,[20] and FMT studies of human stool post-RYGB into GF mice also suggest that the altered microbiome following surgery can lead to decreased adiposity in the recipients,[21] as well as some metabolic improvements.[23] However, direct inferences of the impact of the altered gut microbiome post-surgery have been confounded by the vast individual differences in the composition of gut microbiota among patients pre- and postsurgery. In this study, we used paired samples of patients' stool pre- and post-surgery that were gavaged into WD-fed, GF mice, enabling us to track improvements in metabolic outcomes mediated by the post-surgery microbiota of individual patients. Using this model, we found that alterations in the gut microbiome following RYGB surgery of obese subjects conferred improved metabolic parameters in FMT-colonized, WD-fed mice, independent of body weight and food intake, by primarily increasing brown fat mass and energy expenditure as well as by promoting adipose tissue immune homeostasis. These improvements in abnormal metabolism were causally related to the altered gut microbiota postsurgery, since they were independent of diet and body mass. These observations in mice reflected the improvement in insulin sensitivity that was observed in the three of the four patients.

Host metabolism, as well as systemic inflammation, can have an impact on the gut microbiome composition and function, and in turn, this altered state of the microbiome can have an impact on both the accumulation and the function of adipose tissue[43] and ultimately impacts on the host's energy balance. BAT contributes to energy dissipation through non-shivering thermogenesis, but recent findings have also suggested that BAT activity is linked to a healthier metabolic status independent of weight.[44] This was also reflected in our study, where we found that mice receiving the post-RYGB microbiota exhibited a striking increase in BAT mass and activity and overall increased energy expenditure compared with animals colonized with the presurgery microbiota, despite both groups being on a WD and having similar body weights. These changes may be linked to the increased relative abundances of *A. muciniphila*[45,46] as well as increased levels of short-chain fatty acids (SCFAs)[47] that we observed in some of the mouse cohorts receiving the post-RYGB surgery FMT. SCFAs in particular have been shown to upregulate the expression of UCP1 and PGC1α, concomitantly increasing mitochondrial function and biogenesis in BAT.[48] Understanding the mechanism of how the post-surgery microbiota mediates these changes in the BAT will be of profound interest for future studies.

In terms of white adipose tissue (WAT), immune cells within WAT are associated with a type 2 immune axis, but in obesity and metabolic disease, the immune environment of the WAT shifts toward a more type 1 immune phenotype that is characterized by inflammatory cells and cytokines/adipokines that have deleterious effects on metabolism as well as contributing to systemic inflammation.[49] What was striking in our findings is that, even though body weight and WAT mass were not different between mice receiving pre- or post-surgery FMT, the expression of inflammatory cytokines was decreased, and the expression profile of type 2 immune markers was increased in those mice colonized with the post-surgery microbiota. Moreover, we also found that WAT from mice colonized with post-surgery microbiota showed increased expression levels of *Sirt1*, the gene encoding Sirtuin-1, whose expression has been found to increase in WAT during caloric restriction[50] and also following bariatric surgery.[51] Functionally, Sirtuin-1 plays an important role in metabolic homeostasis by maintaining insulin sensitivity and suppressing inflammation in different tissues.[52] While few data are available to directly link gut microbes to WAT inflammation,[53] a potential mechanism may be through the enhanced abundance of tryptophan-derived metabolites that we observed in mice colonized with the post-RYGB surgery stool. Indeed, recent findings suggest that these microbiota-derived metabolites control expression of the microRNA *miR-181*, whose elevated expression is associated with increased adiposity, insulin resistance, and, importantly, WAT inflammation.[54] Further research is necessary to determine if these metabolites contribute to metabolic health improvements in our model by reducing WAT inflammation.

In the setting of RYGB, vast and durable changes in the microbial community structure and function have been noted postsurgery[21]; however, pinpointing specific compositional and functional changes across cohorts presents a significant challenge. While patient numbers limited us from making generalized conclusions regarding surgery-dependent changes in the microbiota across the individuals in our study, the transfer of paired samples of the patients' stool before and after surgery to two separate cohorts of GF mice enabled us not only to examine diet-independent alterations in the abundance of certain taxa and their functional outputs by metabolomics, but also to correlate these with the metabolic improvements in the animals

(B) Heatmap of the significant differential metabolites in fecal samples of pre- and post-RYGB FMT mice. Color bar indicates the relative abundances of the metabolites, with red indicating a higher concentration and blue indicating a lower concentration (pre n = 15, post n = 14).
(C–F) Relative concentrations of significantly different amino acids (C), tryptophan metabolites (D), short-chain fatty acids (E), and acylcarnitine (F). Each dot represents one mouse/biological replicate (pre n = 15, post n = 14). Data displayed as mean ± SEM. p values were determined using two-tailed unpaired Student's t test. *$p < 0.05$, **$p < 0.005$.

receiving the post-surgery microbiota. In terms of compositional changes, qPCR validated the increase in abundances of *A. muciniphila* (T12 and T41) and *Blautia* spp. (T73 and T79) in the mouse cohorts receiving the post-surgery microbiota compared with mice of the pre-surgery cohorts. These organisms have been associated in previous studies with improvement in both glucose and lipid homeostasis in the setting of T2D and obesity.[55–58,59] The mechanisms by which these microbes improve metabolism are unknown, but *A. muciniphila* is reported to be an indole and SCFA producer, while *Blautia* spp. can produce SCFAs.[60–62] Both of these classes of metabolites were part of the favorable metabolomic changes we observed in the animals receiving the post-surgery microbiota from across the patient cohort (see below).

We observed profound fecal metabolomic changes that may account for the improved metabolic health effects of the post-RYGB microbiota, including increased levels of SCFAs, acylcarnitines, and tryptophan metabolites. SCFAs were previously shown to play important roles in energy metabolism, protection against diet-induced obesity, and regulation of gut hormone secretion, as well as decreasing VAT inflammation and enhancing lipolysis and browning.[63–67] Several long-chain acylcarnitines were also increased in post-RYGB mice, which are known to drive β oxidation in mitochondria and serve as a fuel source for BAT thermogenesis.[68] Consistent with this, higher expression of *Cpt1a*, which is a marker of β-oxidation, was observed in the liver tissue of post-RYGB mice across all patient cohorts (data not shown). Finally, the tryptophan-derived metabolites (indole propionic acid, indole acetic acid, tryptamine, and serotonin) were also increased in the post-RYGB mice, and some of these have been shown to regulate gut hormone secretion, promote gut barrier integrity, reduce inflammation, and improve insulin sensitivity.[69,70]

A number of metabolites were found to be higher in fecal samples of the pre-surgery FMT mouse cohort compared with the post-surgery cohort. These included amino acids (e.g., arginine, glutamic acid, aspartic acid, serine, glycine, glutamine, lysine, and tyrosine), which have been shown to be positively correlated with higher BMI and low physical fitness[71] as well as consumption of a high-fat diet and insulin resistance.[72,73] Higher levels of lactic acid and pyruvate were also observed in the pre-surgery FMT mice compared with the post-surgery cohort, and these have been correlated with systemic and gut inflammation, respectively.[74,75] Notably, while we saw few consistent alterations in taxa within the microbiota pre- and post-surgery in patient stools, nor in the mice colonized with these stools, we were able to uncover possible metabolites that may be causally related to improved metabolic health. Indeed, given the taxonomic variability of the microbiota across patients, the functional capabilities of the metabolites these microbes produce is more likely to be causal in affecting the overall health of the host.[76] For example, different bacterial species within the Firmicutes and Bacteroidetes phyla can ferment dietary fiber to SCFAs, which have a number of health benefits, including signaling through GPCRs to induced satiety. Future work will be required to determine how these metabolites may be altering systemic changes in the post-surgery recipient mice in terms of improved glucose handling, WAT homeostasis, and energy expenditure.

In summary, our approach enabled the pairwise comparison of metabolic outcomes of mice receiving FMT from individual obese patients pre- and post-RYGB surgery. In mice colonized with the post-surgery microbiota, we observed diet- and weight-independent improvements in glucose handing and insulin sensitivity, energy expenditure, and BAT activity, as well as diminished WAT inflammation. These studies provide evidence for a direct role of RYGB-dependent alterations in the gut microbiota and their associated metabolites in improved metabolic health and will pave the way for future work to explore what functional aspects of the microbiota are responsible for these improvements. Moreover, these findings encourage targeted pre- or probiotic approaches as well as the consideration of healthy FMTs as a means to treat obesity and avoid the need for surgical intervention.

Limitations of the study

While this work supports the conclusion that RYGB surgery imposes changes to the gut microbiome that lead to metabolic improvements in the host, there are some limitations of our study. First, an acknowledged limitation is that only a subset (four patients) of the larger patient group was examined. Second, individual mouse cohorts receiving patient FMTs have been proposed to be viewed as "pseudoreplicates"[77]; this is acknowledged to a certain extent in our study; however, each paired patient sample was transferred to two different cohorts of mice that were separated by more than a year between experiments, thereby supporting the robustness of the experimental outcome. Related to this, while past FMT studies on GF mice used normal chow diet, in our study mice colonized with pre- and post-surgery microbiota were maintained on a WD. By using the WD, we reasoned that we might be able to identify more significant, health-promoting microbes/metabolites that have the potential to be used as therapeutic strategies in obese patients regardless of the individual's diet. We plan to test this idea in future studies. Finally, while metagenomic sequencing, rather than 16S rRNA amplicon sequencing would have likely uncovered more significant taxonomic and possibly potential functional differences between the pre- and the post-surgery transplanted microbiota, we expected that 16S rRNA sequencing coupled with metabolomics was an appropriate approach to discern functional effects of the gut microbiome, which are thought to be more relevant for affecting health.[76]

STAR★METHODS

Detailed methods are provided in the online version of this paper and include the following:

- KEY RESOURCES TABLE
- RESOURCE AVAILABILITY
  - Lead contact
  - Materials availability
  - Data and code availability
- EXPERIMENTAL MODEL AND SUBJECT DETAILS
  - Human participants
  - Faecal sample collection
  - Preparation of patient fecal samples

SUPPLEMENTAL INFORMATION

Supplemental information can be found online at https://doi.org/10.1016/j.xcrm.2023.101051.

ACKNOWLEDGMENTS

The authors would like to acknowledge funding for this project from the Canadian Institute for Health Research (CIHR) team grant TB2-138775 to J.P.A. and H.Y.G. J.Y. was supported by a postdoctoral fellowship from the Banting and Best Diabetes Centre (BBDC), University of Toronto. N.N. was supported by a studentship from the BBDC. We thank the Temerty Faculty of Medicine, Department of Comparative Medicine's Germ-Free Facility at the University of Toronto, especially Karen Parisienne, Elaine Tam, Amy Cao, Laura Kent, and Stacy Nichols; the Spatio-Temporal Targeting and Amplification of Radiation Response (STTARR) Innovation Centre and its affiliated funding agencies, especially Deborah Scollard and Teesha Komal; the Centre for Analysis of Genome Evolution & Function (CAGEF), especially Pauline Wang and Sylva Donaldson, for DNA sequencing; as well as The Metabolomics Innovation Centre (TMIC), University of Alberta. Finally, we thank the patients and their families for participating in this research.

AUTHOR CONTRIBUTIONS

J.Y., T.L., and T.Q carried out the experiments and interpreted the data. N.N. analyzed the mouse metabolite data. K.J.P.S., A.O., and T.J. contributed to subject recruitment; K.J.P.S. performed sample processing and clinical data analysis; L.P. performed the CellProfiler analysis. L.X. did the pancreatic islet cell analysis. H.L., D.A.W., and M.W. performed the metabolic cage study. H.M. analyzed the 16S rRNA gene amplicon sequencing data. W.L. helped with the statistical analysis. K.B. developed the animal FMT protocol. S.S.H. and S.M.P. prepared human patient FMT filtrates. D.J.P., S.J.R., J.P.A., and H.Y.G. designed the study and methodology. J.Y., H.Y.G., and D.J.P. wrote the manuscript. H.-K.S., J.P.A., H.Y.G., and D.J.P. revised the manuscript. All authors approved the final version of the manuscript.

DECLARATION OF INTERESTS

The authors declare no competing interests.

INCLUSION AND DIVERSITY

We worked to ensure gender balance in the recruitment of human subjects. We worked to ensure ethnic or other types of diversity in the recruitment of human subjects. We worked to ensure that the study questionnaires were prepared in an inclusive way. We avoided "helicopter science" practices by including the participating local contributors from the region where we conducted the research as authors on the paper.

Received: July 18, 2022
Revised: December 20, 2022
Accepted: April 21, 2023
Published: May 16, 2023

REFERENCES

1. Buchwald, H., Avidor, Y., Braunwald, E., Jensen, M.D., Pories, W., Fahrbach, K., and Schoelles, K. (2004). Bariatric surgery: a systematic review and meta-analysis. JAMA *292*, 1724–1737. https://doi.org/10.1001/jama.292.14.1724.
2. Schauer, P.R., Bhatt, D.L., Kirwan, J.P., Wolski, K., Brethauer, S.A., Navaneethan, S.D., Aminian, A., Pothier, C.E., Kim, E.S.H., Nissen, S.E., et al. (2014). Bariatric surgery versus intensive medical therapy for diabetes–3-year outcomes. N. Engl. J. Med. *370*, 2002–2013. https://doi.org/10.1056/NEJMoa1401329.
3. Sjöström, L., Narbro, K., Sjöström, C.D., Karason, K., Larsson, B., Wedel, H., Lystig, T., Sullivan, M., Bouchard, C., Carlsson, B., et al. (2007). Effects of bariatric surgery on mortality in Swedish obese subjects. N. Engl. J. Med. *357*, 741–752. https://doi.org/10.1056/NEJMoa066254.
4. Jørgensen, N.B., Dirksen, C., Bojsen-Møller, K.N., Jacobsen, S.H., Worm, D., Hansen, D.L., Kristiansen, V.B., Naver, L., Madsbad, S., and Holst, J.J. (2013). Exaggerated glucagon-like peptide 1 response is important for improved beta-cell function and glucose tolerance after Roux-en-Y gastric bypass in patients with type 2 diabetes. Diabetes *62*, 3044–3052. https://doi.org/10.2337/db13-0022.
5. Habib, A.M., Richards, P., Rogers, G.J., Reimann, F., and Gribble, F.M. (2013). Co-localisation and secretion of glucagon-like peptide 1 and peptide YY from primary cultured human L cells. Diabetologia *56*, 1413–1416. https://doi.org/10.1007/s00125-013-2887-z.
6. Guida, C., Stephen, S.D., Watson, M., Dempster, N., Larraufie, P., Marjot, T., Cargill, T., Rickers, L., Pavlides, M., Tomlinson, J., et al. (2019). PYY plays a key role in the resolution of diabetes following bariatric surgery in humans. EBioMedicine *40*, 67–76. https://doi.org/10.1016/j.ebiom.2018.12.040.
7. Amouyal, C., Castel, J., Guay, C., Lacombe, A., Denom, J., Migrenne-Li, S., Rouault, C., Marquet, F., Georgiadou, E., Stylianides, T., et al. (2020). A surrogate of Roux-en-Y gastric bypass (the enterogastro anastomosis surgery) regulates multiple beta-cell pathways during resolution of diabetes in ob/ob mice. EBioMedicine *58*, 102895. https://doi.org/10.1016/j.ebiom.2020.102895.
8. Batterham, R.L., Cohen, M.A., Ellis, S.M., Le Roux, C.W., Withers, D.J., Frost, G.S., Ghatei, M.A., and Bloom, S.R. (2003). Inhibition of food intake in obese subjects by peptide YY3-36. N. Engl. J. Med. *349*, 941–948. https://doi.org/10.1056/NEJMoa030204.
9. Scrocchi, L.A., Brown, T.J., MaClusky, N., Brubaker, P.L., Auerbach, A.B., Joyner, A.L., and Drucker, D.J. (1996). Glucose intolerance but normal satiety in mice with a null mutation in the glucagon-like peptide 1 receptor gene. Nat. Med. *2*, 1254–1258. https://doi.org/10.1038/nm1196-1254.
10. Breen, D.M., Rasmussen, B.A., Kokorovic, A., Wang, R., Cheung, G.W.C., and Lam, T.K.T. (2012). Jejunal nutrient sensing is required for duodenal-jejunal bypass surgery to rapidly lower glucose concentrations in uncontrolled diabetes. Nat. Med. *18*, 950–955. https://doi.org/10.1038/nm.2745.
11. Wahlström, A., Sayin, S.I., Marschall, H.U., and Bäckhed, F. (2016). Intestinal crosstalk between bile acids and microbiota and its impact on host metabolism. Cell Metab. *24*, 41–50. https://doi.org/10.1016/j.cmet.2016.05.005.
12. Aron-Wisnewsky, J., Doré, J., and Clement, K. (2012). The importance of the gut microbiota after bariatric surgery. Nat. Rev. Gastroenterol. Hepatol. *9*, 590–598. https://doi.org/10.1038/nrgastro.2012.161.
13. Zhang, H., DiBaise, J.K., Zuccolo, A., Kudrna, D., Braidotti, M., Yu, Y., Parameswaran, P., Crowell, M.D., Wing, R., Rittmann, B.E., and Krajmalnik-Brown, R. (2009). Human gut microbiota in obesity and after gastric bypass. Proc. Natl. Acad. Sci. USA *106*, 2365–2370. https://doi.org/10.1073/pnas.0812600106.
14. Bäckhed, F., Ding, H., Wang, T., Hooper, L.V., Koh, G.Y., Nagy, A., Semenkovich, C.F., and Gordon, J.I. (2004). The gut microbiota as an

environmental factor that regulates fat storage. Proc. Natl. Acad. Sci. USA *101*, 15718–15723. https://doi.org/10.1073/pnas.0407076101.

15. Turnbaugh, P.J., Ley, R.E., Mahowald, M.A., Magrini, V., Mardis, E.R., and Gordon, J.I. (2006). An obesity-associated gut microbiome with increased capacity for energy harvest. Nature *444*, 1027–1031. https://doi.org/10.1038/nature05414.
16. Ley, R.E., Bäckhed, F., Turnbaugh, P., Lozupone, C.A., Knight, R.D., and Gordon, J.I. (2005). Obesity alters gut microbial ecology. Proc. Natl. Acad. Sci. USA *102*, 11070–11075. https://doi.org/10.1073/pnas.0504978102.
17. Ridaura, V.K., Faith, J.J., Rey, F.E., Cheng, J., Duncan, A.E., Kau, A.L., Griffin, N.W., Lombard, V., Henrissat, B., Bain, J.R., et al. (2013). Gut microbiota from twins discordant for obesity modulate metabolism in mice. Science *341*, 1241214. https://doi.org/10.1126/science.1241214.
18. Turnbaugh, P.J., Bäckhed, F., Fulton, L., and Gordon, J.I. (2008). Diet-induced obesity is linked to marked but reversible alterations in the mouse distal gut microbiome. Cell Host Microbe *3*, 213–223. https://doi.org/10.1016/j.chom.2008.02.015.
19. Turnbaugh, P.J., Ridaura, V.K., Faith, J.J., Rey, F.E., Knight, R., and Gordon, J.I. (2009). The effect of diet on the human gut microbiome: a metagenomic analysis in humanized gnotobiotic mice. Sci. Transl. Med. *1*, 6ra14. https://doi.org/10.1126/scitranslmed.3000322.
20. Liou, A.P., Paziuk, M., Luevano, J.M., Jr., Machineni, S., Turnbaugh, P.J., and Kaplan, L.M. (2013). Conserved shifts in the gut microbiota due to gastric bypass reduce host weight and adiposity. Sci. Transl. Med. *5*, 178ra41. https://doi.org/10.1126/scitranslmed.3005687.
21. Tremaroli, V., Karlsson, F., Werling, M., Ståhlman, M., Kovatcheva-Datchary, P., Olbers, T., Fändriks, L., le Roux, C.W., Nielsen, J., and Bäckhed, F. (2015). Roux-en-Y gastric bypass and vertical banded gastroplasty induce long-term changes on the human gut microbiome contributing to fat mass regulation. Cell Metab. *22*, 228–238. https://doi.org/10.1016/j.cmet.2015.07.009.
22. Debédat, J., Le Roy, T., Voland, L., Belda, E., Alili, R., Adriouch, S., Bel Lassen, P., Kasahara, K., Hutchison, E., Genser, L., et al. (2022). The human gut microbiota contributes to type-2 diabetes non-resolution 5-years after Roux-en-Y gastric bypass. Gut Microb. *14*, 2050635. https://doi.org/10.1080/19490976.2022.2050635.
23. Anhê, F.F., Zlitni, S., Zhang, S.Y., Choi, B.S., Chen, C.Y., Foley, K.P., Barra, N.G., Surette, M.G., Biertho, L., Richard, D., et al. (2022). Human gut microbiota after bariatric surgery alters intestinal morphology and glucose absorption in mice independently of obesity. Gut *72*, 460–471. https://doi.org/10.1136/gutjnl-2022-328185.
24. Beltran Del Rio, M., Tiwari, M., Amodu, L.I., Cagliani, J., and Rodriguez Rilo, H.L. (2016). Glycated hemoglobin, plasma glucose, and erythrocyte aging. J. Diabetes Sci. Technol. *10*, 1303–1307. https://doi.org/10.1177/1932296816659885.
25. Schwenger, K.J.P., Fischer, S.E., Jackson, T.D., Okrainec, A., and Allard, J.P. (2018). Non-alcoholic fatty liver disease in morbidly obese individuals undergoing bariatric surgery: prevalence and effect of the pre-bariatric very low calorie diet. Obes. Surg. *28*, 1109–1116. https://doi.org/10.1007/s11695-017-2980-3.
26. Schwenger, K.J.P., Fischer, S.E., Jackson, T., Okrainec, A., and Allard, J.P. (2018). In nonalcoholic fatty liver disease, Roux-en-Y gastric bypass improves liver histology while persistent disease is associated with lower improvements in waist circumference and glycemic control. Surg. Obes. Relat. Dis. *14*, 1233–1239. https://doi.org/10.1016/j.soard.2018.06.007.
27. Zhang, A.M.Y., Wellberg, E.A., Kopp, J.L., and Johnson, J.D. (2021). Hyperinsulinemia in obesity, inflammation, and cancer. Diabetes Metab. J. *45*, 285–311. https://doi.org/10.4093/dmj.2020.0250.
28. Cannon, B., and Nedergaard, J. (2004). Brown adipose tissue: function and physiological significance. Physiol. Rev. *84*, 277–359. https://doi.org/10.1152/physrev.00015.2003.
29. Zhang, F., Hao, G., Shao, M., Nham, K., An, Y., Wang, Q., Zhu, Y., Kusminski, C.M., Hassan, G., Gupta, R.K., et al. (2018). An adipose tissue atlas: an image-guided identification of human-like BAT and beige depots in rodents. Cell Metab. *27*, 252–262.e3. https://doi.org/10.1016/j.cmet.2017.12.004.
30. Cypess, A.M., White, A.P., Vernochet, C., Schulz, T.J., Xue, R., Sass, C.A., Huang, T.L., Roberts-Toler, C., Weiner, L.S., Sze, C., et al. (2013). Anatomical localization, gene expression profiling and functional characterization of adult human neck brown fat. Nat. Med. *19*, 635–639. https://doi.org/10.1038/nm.3112.
31. Blüher, M. (2016). Adipose tissue inflammation: a cause or consequence of obesity-related insulin resistance? Clin. Sci. *130*, 1603–1614. https://doi.org/10.1042/CS20160005.
32. Xu, H., Barnes, G.T., Yang, Q., Tan, G., Yang, D., Chou, C.J., Sole, J., Nichols, A., Ross, J.S., Tartaglia, L.A., and Chen, H. (2003). Chronic inflammation in fat plays a crucial role in the development of obesity-related insulin resistance. J. Clin. Invest. *112*, 1821–1830. https://doi.org/10.1172/JCI19451.
33. Man, K., Kallies, A., and Vasanthakumar, A. (2022). Resident and migratory adipose immune cells control systemic metabolism and thermogenesis. Cell. Mol. Immunol. *19*, 421–431. https://doi.org/10.1038/s41423-021-00804-7.
34. Yeung, F., Hoberg, J.E., Ramsey, C.S., Keller, M.D., Jones, D.R., Frye, R.A., and Mayo, M.W. (2004). Modulation of NF-kappaB-dependent transcription and cell survival by the SIRT1 deacetylase. EMBO J. *23*, 2369–2380. https://doi.org/10.1038/sj.emboj.7600244.
35. Gillum, M.P., Kotas, M.E., Erion, D.M., Kursawe, R., Chatterjee, P., Nead, K.T., Muise, E.S., Hsiao, J.J., Frederick, D.W., Yonemitsu, S., et al. (2011). SirT1 regulates adipose tissue inflammation. Diabetes *60*, 3235–3245. https://doi.org/10.2337/db11-0616.
36. Pfluger, P.T., Herranz, D., Velasco-Miguel, S., Serrano, M., and Tschöp, M.H. (2008). Sirt1 protects against high-fat diet-induced metabolic damage. Proc. Natl. Acad. Sci. USA *105*, 9793–9798. https://doi.org/10.1073/pnas.0802917105.
37. Becker, M., Levings, M.K., and Daniel, C. (2017). Adipose-tissue regulatory T cells: critical players in adipose-immune crosstalk. Eur. J. Immunol. *47*, 1867–1874. https://doi.org/10.1002/eji.201646739.
38. Kolodin, D., van Panhuys, N., Li, C., Magnuson, A.M., Cipolletta, D., Miller, C.M., Wagers, A., Germain, R.N., Benoist, C., and Mathis, D. (2015). Antigen- and cytokine-driven accumulation of regulatory T cells in visceral adipose tissue of lean mice. Cell Metab. *21*, 543–557. https://doi.org/10.1016/j.cmet.2015.03.005.
39. Molofsky, A.B., Nussbaum, J.C., Liang, H.E., Van Dyken, S.J., Cheng, L.E., Mohapatra, A., Chawla, A., and Locksley, R.M. (2013). Innate lymphoid type 2 cells sustain visceral adipose tissue eosinophils and alternatively activated macrophages. J. Exp. Med. *210*, 535–549. https://doi.org/10.1084/jem.20121964.
40. Molofsky, A.B., Savage, A.K., and Locksley, R.M. (2015). Interleukin-33 in tissue homeostasis, injury, and inflammation. Immunity *42*, 1005–1019. https://doi.org/10.1016/j.immuni.2015.06.006.
41. Velazquez-Villegas, L.A., Perino, A., Lemos, V., Zietak, M., Nomura, M., Pols, T.W.H., and Schoonjans, K. (2018). TGR5 signalling promotes mitochondrial fission and beige remodelling of white adipose tissue. Nat. Commun. *9*, 245. https://doi.org/10.1038/s41467-017-02068-0.
42. Reed, M.A., Pories, W.J., Chapman, W., Pender, J., Bowden, R., Barakat, H., Gavin, T.P., Green, T., Tapscott, E., Zheng, D., et al. (2011). Roux-en-Y gastric bypass corrects hyperinsulinemia implications for the remission of type 2 diabetes. J. Clin. Endocrinol. Metab. *96*, 2525–2531. https://doi.org/10.1210/jc.2011-0165.
43. Moreno-Navarrete, J.M., and Fernandez-Real, J.M. (2019). The gut microbiota modulates both browning of white adipose tissue and the activity of brown adipose tissue. Rev. Endocr. Metab. Disord. *20*, 387–397. https://doi.org/10.1007/s11154-019-09523-x.
44. Herz, C.T., Kulterer, O.C., Prager, M., Schmöltzer, C., Langer, F.B., Prager, G., Marculescu, R., Kautzky-Willer, A., Hacker, M., Haug, A.R., and Kiefer, F.W. (2021). Active Brown adipose tissue is associated with

a healthier metabolic phenotype in obesity. Diabetes *71*, 93–103. https://doi.org/10.2337/db21-0475.

45. Depommier, C., Van Hul, M., Everard, A., Delzenne, N.M., De Vos, W.M., and Cani, P.D. (2020). Pasteurized Akkermansia muciniphila increases whole-body energy expenditure and fecal energy excretion in diet-induced obese mice. Gut Microb. *11*, 1231–1245. https://doi.org/10.1080/19490976.2020.1737307.
46. Yoon, H.S., Cho, C.H., Yun, M.S., Jang, S.J., You, H.J., Kim, J.H., Han, D., Cha, K.H., Moon, S.H., Lee, K., et al. (2021). Akkermansia muciniphila secretes a glucagon-like peptide-1-inducing protein that improves glucose homeostasis and ameliorates metabolic disease in mice. Nat. Microbiol. *6*, 563–573. https://doi.org/10.1038/s41564-021-00880-5.
47. Sukkar, A.H., Lett, A.M., Frost, G., and Chambers, E.S. (2019). Regulation of energy expenditure and substrate oxidation by short-chain fatty acids. J. Endocrinol. *242*, R1–R8. https://doi.org/10.1530/JOE-19-0098.
48. Gao, Z., Yin, J., Zhang, J., Ward, R.E., Martin, R.J., Lefevre, M., Cefalu, W.T., and Ye, J. (2009). Butyrate improves insulin sensitivity and increases energy expenditure in mice. Diabetes *58*, 1509–1517. https://doi.org/10.2337/db08-1637.
49. Michailidou, Z., Gomez-Salazar, M., and Alexaki, V.I. (2022). Innate immune cells in the adipose tissue in health and metabolic disease. J. Innate Immun. *14*, 4–30. https://doi.org/10.1159/000515117.
50. Quiñones, M., Al-Massadi, O., Fernø, J., and Nogueiras, R. (2014). Cross-talk between SIRT1 and endocrine factors: effects on energy homeostasis. Mol. Cell. Endocrinol. *397*, 42–50. https://doi.org/10.1016/j.mce.2014.08.002.
51. Ferraz-Bannitz, R., Welendorf, C.R., Coelho, P.O., Salgado, W., Jr., Nonino, C.B., Beraldo, R.A., and Foss-Freitas, M.C. (2021). Bariatric surgery can acutely modulate ER-stress and inflammation on subcutaneous adipose tissue in non-diabetic patients with obesity. Diabetol. Metab. Syndr. *13*, 19. https://doi.org/10.1186/s13098-021-00623-w.
52. Kitada, M., Ogura, Y., Monno, I., and Koya, D. (2019). Sirtuins and type 2 diabetes: role in inflammation, oxidative stress, and mitochondrial function. Front. Endocrinol. *10*, 187. https://doi.org/10.3389/fendo.2019.00187.
53. Tran, H.Q., Bretin, A., Adeshirlarijaney, A., Yeoh, B.S., Vijay-Kumar, M., Zou, J., Denning, T.L., Chassaing, B., and Gewirtz, A.T. (2020). Western diet"-induced adipose inflammation requires a complex gut microbiota. Cell. Mol. Gastroenterol. Hepatol. *9*, 313–333. https://doi.org/10.1016/j.jcmgh.2019.09.009.
54. Virtue, A.T., McCright, S.J., Wright, J.M., Jimenez, M.T., Mowel, W.K., Kotzin, J.J., Joannas, L., Basavappa, M.G., Spencer, S.P., Clark, M.L., et al. (2019). The gut microbiota regulates white adipose tissue inflammation and obesity via a family of microRNAs. Sci. Transl. Med. *11*, eaav1892. https://doi.org/10.1126/scitranslmed.aav1892.
55. Cani, P.D., and de Vos, W.M. (2017). Next-generation beneficial microbes: the case of Akkermansia muciniphila. Front. Microbiol. *8*, 1765. https://doi.org/10.3389/fmicb.2017.01765.
56. Plovier, H., Everard, A., Druart, C., Depommier, C., Van Hul, M., Geurts, L., Chilloux, J., Ottman, N., Duparc, T., Lichtenstein, L., et al. (2017). A purified membrane protein from Akkermansia muciniphila or the pasteurized bacterium improves metabolism in obese and diabetic mice. Nat. Med. *23*, 107–113. https://doi.org/10.1038/nm.4236.
57. Schneeberger, M., Everard, A., Gómez-Valadés, A.G., Matamoros, S., Ramírez, S., Delzenne, N.M., Gomis, R., Claret, M., and Cani, P.D. (2015). Akkermansia muciniphila inversely correlates with the onset of inflammation, altered adipose tissue metabolism and metabolic disorders during obesity in mice. Sci. Rep. *5*, 16643. https://doi.org/10.1038/srep16643.
58. Tong, X., Xu, J., Lian, F., Yu, X., Zhao, Y., Xu, L., Zhang, M., Zhao, X., Shen, J., Wu, S., et al. (2018). Structural alteration of gut microbiota during the amelioration of human type 2 diabetes with hyperlipidemia by metformin and a traditional Chinese herbal formula: a multicenter, randomized, open label clinical trial. mBio *9*, e02392-17. https://doi.org/10.1128/mBio.02392-17.
59. Benitez-Paez, A., Gomez Del Pugar, E.M., Lopez-Almela, I., Moya-Perez, A., Codoner-Franch, P., and Sanz, Y. (2020). Depletion of Blautia species in the microbiota of obese children relates to intestinal inflammation and metabolic phenotype worsening. mSystems *5*, e00857-19. https://doi.org/10.1128/mSystems.00857-19.
60. Cani, P.D., Depommier, C., Derrien, M., Everard, A., and de Vos, W.M. (2022). Akkermansia muciniphila: paradigm for next-generation beneficial microorganisms. Nat. Rev. Gastroenterol. Hepatol. *19*, 625–637. https://doi.org/10.1038/s41575-022-00631-9.
61. Liu, X., Mao, B., Gu, J., Wu, J., Cui, S., Wang, G., Zhao, J., Zhang, H., and Chen, W. (2021). Blautia-a new functional genus with potential probiotic properties? Gut Microb. *13*, 1–21. https://doi.org/10.1080/19490976.2021.1875796.
62. Yin, J., Song, Y., Hu, Y., Wang, Y., Zhang, B., Wang, J., Ji, X., and Wang, S. (2021). Dose-dependent beneficial effects of tryptophan and its derived metabolites on Akkermansia in vitro: a preliminary prospective study. Microorganisms *9*, 1511. https://doi.org/10.3390/microorganisms9071511.
63. Al-Lahham, S., Roelofsen, H., Rezaee, F., Weening, D., Hoek, A., Vonk, R., and Venema, K. (2012). Propionic acid affects immune status and metabolism in adipose tissue from overweight subjects. Eur. J. Clin. Invest. *42*, 357–364. https://doi.org/10.1111/j.1365-2362.2011.02590.x.
64. Cummings, J.H. (1981). Short chain fatty acids in the human colon. Gut *22*, 763–779. https://doi.org/10.1136/gut.22.9.763.
65. De Vadder, F., Kovatcheva-Datchary, P., Goncalves, D., Vinera, J., Zitoun, C., Duchampt, A., Bäckhed, F., and Mithieux, G. (2014). Microbiota-generated metabolites promote metabolic benefits via gut-brain neural circuits. Cell *156*, 84–96. https://doi.org/10.1016/j.cell.2013.12.016.
66. Lin, H.V., Frassetto, A., Kowalik, E.J., Jr., Nawrocki, A.R., Lu, M.M., Kosinski, J.R., Hubert, J.A., Szeto, D., Yao, X., Forrest, G., and Marsh, D.J. (2012). Butyrate and propionate protect against diet-induced obesity and regulate gut hormones via free fatty acid receptor 3-independent mechanisms. PLoS One *7*, e35240. https://doi.org/10.1371/journal.pone.0035240.
67. May, K.S., and den Hartigh, L.J. (2021). Modulation of adipocyte metabolism by microbial short-chain fatty acids. Nutrients *13*, 3666. https://doi.org/10.3390/nu13103666.
68. Simcox, J., Geoghegan, G., Maschek, J.A., Bensard, C.L., Pasquali, M., Miao, R., Lee, S., Jiang, L., Huck, I., Kershaw, E.E., et al. (2017). Global analysis of plasma lipids identifies liver-derived acylcarnitines as a fuel source for Brown fat thermogenesis. Cell Metab. *26*, 509–522.e6. https://doi.org/10.1016/j.cmet.2017.08.006.
69. Hu, W., Yan, G., Ding, Q., Cai, J., Zhang, Z., Zhao, Z., Lei, H., and Zhu, Y.Z. (2022). Update of Indoles: promising molecules for ameliorating metabolic diseases. Biomed. Pharmacother. *150*, 112957. https://doi.org/10.1016/j.biopha.2022.112957.
70. Koh, A., and Bäckhed, F. (2020). From association to causality: the role of the gut microbiota and its functional products on host metabolism. Mol. Cell *78*, 584–596. https://doi.org/10.1016/j.molcel.2020.03.005.
71. Cui, M., Trimigno, A., Castro-Mejía, J.L., Reitelseder, S., Bülow, J., Bechshøft, R.L., Nielsen, D.S., Holm, L., Engelsen, S.B., and Khakimov, B. (2021). Human fecal metabolome reflects differences in body mass index, physical fitness, and blood lipoproteins in healthy older adults. Metabolites *11*, 717. https://doi.org/10.3390/metabo11110717.
72. Wang, T.J., Larson, M.G., Vasan, R.S., Cheng, S., Rhee, E.P., McCabe, E., Lewis, G.D., Fox, C.S., Jacques, P.F., Fernandez, C., et al. (2011). Metabolite profiles and the risk of developing diabetes. Nat. Med. *17*, 448–453. https://doi.org/10.1038/nm.2307.
73. Lin, H., An, Y., Hao, F., Wang, Y., and Tang, H. (2016). Correlations of fecal metabonomic and microbiomic changes induced by high-fat diet in the pre-obesity state. Sci. Rep. *6*, 21618. https://doi.org/10.1038/srep21618.
74. Tiihonen, K., Ouwehand, A.C., and Rautonen, N. (2010). Effect of overweight on gastrointestinal microbiology and immunology: correlation

with blood biomarkers. Br. J. Nutr. *103*, 1070–1078. https://doi.org/10.1017/S0007114509992807.

75. Huda-Faujan, N., Abdulamir, A.S., Fatimah, A.B., Anas, O.M., Shuhaimi, M., Yazid, A.M., and Loong, Y.Y. (2010). The impact of the level of the intestinal short chain fatty acids in inflammatory bowel disease patients versus healthy subjects. Open Biochem. J. *4*, 53–58. https://doi.org/10.2174/1874091X01004010053.
76. Fan, Y., and Pedersen, O. (2021). Gut microbiota in human metabolic health and disease. Nat. Rev. Microbiol. *19*, 55–71. https://doi.org/10.1038/s41579-020-0433-9.
77. Walter, J., Armet, A.M., Finlay, B.B., and Shanahan, F. (2020). Establishing or exaggerating causality for the gut microbiome: lessons from human microbiota-associated rodents. Cell *180*, 221–232. https://doi.org/10.1016/j.cell.2019.12.025.
78. (1991). NIH conference. Gastrointestinal surgery for severe obesity. Consensus Development Conference Panel. Ann. Intern. Med. *115*, 956–961.
79. Matthews, D.R., Hosker, J.P., Rudenski, A.S., Naylor, B.A., Treacher, D.F., and Turner, R.C. (1985). Homeostasis model assessment: insulin resistance and beta-cell function from fasting plasma glucose and insulin concentrations in man. Diabetologia *28*, 412–419. https://doi.org/10.1007/BF00280883.
80. Ghorbani, Y., Schwenger, K.J.P., Sharma, D., Jung, H., Yadav, J., Xu, W., Lou, W., Poutanen, S., Hota, S.S., Comelli, E.M., et al. (2023). Effect of faecal microbial transplant via colonoscopy in patients with severe obesity and insulin resistance: a randomized double-blind, placebo-controlled Phase 2 trial. Diabetes Obes. Metab. *25*, 479–490. https://doi.org/10.1111/dom.14891.
81. Qin, J., Li, R., Raes, J., Arumugam, M., Burgdorf, K.S., Manichanh, C., Nielsen, T., Pons, N., Levenez, F., Yamada, T., et al. (2010). A human gut microbial gene catalogue established by metagenomic sequencing. Nature *464*, 59–65. https://doi.org/10.1038/nature08821.
82. Da Silva, H.E., Teterina, A., Comelli, E.M., Taibi, A., Arendt, B.M., Fischer, S.E., Lou, W., and Allard, J.P. (2018). Nonalcoholic fatty liver disease is associated with dysbiosis independent of body mass index and insulin resistance. Sci. Rep. *8*, 1466. https://doi.org/10.1038/s41598-018-19753-9.
83. Liang, T., Qin, T., Kang, F., Kang, Y., Xie, L., Zhu, D., Dolai, S., Greitzer-Antes, D., Baker, R.K., Feng, D., et al. (2020). SNAP23 depletion enables more SNAP25/calcium channel excitosome formation to increase insulin exocytosis in type 2 diabetes. JCI Insight *5*, e129694. https://doi.org/10.1172/jci.insight.129694.
84. Wang, X., Minze, L.J., and Shi, Z.Z. (2012). Functional imaging of brown fat in mice with 18F-FDG micro-PET/CT. J. Vis. Exp., 4060. https://doi.org/10.3791/4060.
85. Revelo, X.S., Tsai, S., Lei, H., Luck, H., Ghazarian, M., Tsui, H., Shi, S.Y., Schroer, S., Luk, C.T., Lin, G.H.Y., et al. (2015). Perforin is a novel immune regulator of obesity-related insulin resistance. Diabetes *64*, 90–103. https://doi.org/10.2337/db13-1524.
86. Tschöp, M.H., Speakman, J.R., Arch, J.R.S., Auwerx, J., Brüning, J.C., Chan, L., Eckel, R.H., Farese, R.V., Jr., Galgani, J.E., Hambly, C., et al. (2011). A guide to analysis of mouse energy metabolism. Nat. Methods *9*, 57–63. https://doi.org/10.1038/nmeth.1806.
87. Zhu, D., Zhang, Y., Lam, P.P.L., Dolai, S., Liu, Y., Cai, E.P., Choi, D., Schroer, S.A., Kang, Y., Allister, E.M., et al. (2012). Dual role of VAMP8 in regulating insulin exocytosis and islet beta cell growth. Cell Metab. *16*, 238–249. https://doi.org/10.1016/j.cmet.2012.07.001.
88. Cirera, S. (2013). Highly efficient method for isolation of total RNA from adipose tissue. BMC Res. Notes *6*, 472. https://doi.org/10.1186/1756-0500-6-472.
89. Caporaso, J.G., Lauber, C.L., Walters, W.A., Berg-Lyons, D., Huntley, J., Fierer, N., Owens, S.M., Betley, J., Fraser, L., Bauer, M., et al. (2012). Ultra-high-throughput microbial community analysis on the Illumina HiSeq and MiSeq platforms. ISME J. *6*, 1621–1624. https://doi.org/10.1038/ismej.2012.8.
90. Robertson, S.J., Zhou, J.Y., Geddes, K., Rubino, S.J., Cho, J.H., Girardin, S.E., and Philpott, D.J. (2013). Nod1 and Nod2 signaling does not alter the composition of intestinal bacterial communities at homeostasis. Gut Microb. *4*, 222–231. https://doi.org/10.4161/gmic.24373.
91. Zheng, J., Zhang, L., Johnson, M., Mandal, R., and Wishart, D.S. (2020). Comprehensive targeted metabolomic assay for urine analysis. Anal. Chem. *92*, 10627–10634. https://doi.org/10.1021/acs.analchem.0c01682.
92. López-Hernández, Y., Monárrez-Espino, J., Oostdam, A.H., Delgado, J.E.C., Zhang, L., Zheng, J., Valdez, J.J.O., Mandal, R., González, F.d.L.O., Moreno, J.C.B., et al. (2021). Targeted metabolomics identifies high performing diagnostic and prognostic biomarkers for COVID-19. Sci. Rep. *11*, 14732. https://doi.org/10.1038/s41598-021-94171-y.
93. Edgar, R.C. (2013). UPARSE: highly accurate OTU sequences from microbial amplicon reads. Nat. Methods *10*, 996–998. https://doi.org/10.1038/nmeth.2604.
94. Edgar, R.C. (2010). Search and clustering orders of magnitude faster than BLAST. Bioinformatics *26*, 2460–2461. https://doi.org/10.1093/bioinformatics/btq461.
95. Rognes, T., Flouri, T., Nichols, B., Quince, C., and Mahé, F. (2016). VSEARCH: a versatile open source tool for metagenomics. PeerJ *4*, e2584. https://doi.org/10.7717/peerj.2584.
96. Wang, Q., Garrity, G.M., Tiedje, J.M., and Cole, J.R. (2007). Naive Bayesian classifier for rapid assignment of rRNA sequences into the new bacterial taxonomy. Appl. Environ. Microbiol. *73*, 5261–5267. https://doi.org/10.1128/AEM.00062-07.
97. Caporaso, J.G., Kuczynski, J., Stombaugh, J., Bittinger, K., Bushman, F.D., Costello, E.K., Fierer, N., Peña, A.G., Goodrich, J.K., Gordon, J.I., et al. (2010). QIIME allows analysis of high-throughput community sequencing data. Nat. Methods *7*, 335–336. https://doi.org/10.1038/nmeth.f.303.
98. Mandal, S., Van Treuren, W., White, R.A., Eggesbø, M., Knight, R., and Peddada, S.D. (2015). Analysis of composition of microbiomes: a novel method for studying microbial composition. Microb. Ecol. Health Dis. *26*, 27663. https://doi.org/10.3402/mehd.v26.27663.
99. Bolyen, E., Rideout, J.R., Dillon, M.R., Bokulich, N.A., Abnet, C.C., Al-Ghalith, G.A., Alexander, H., Alm, E.J., Arumugam, M., Asnicar, F., et al. (2019). Reproducible, interactive, scalable and extensible microbiome data science using QIIME 2. Nat. Biotechnol. *37*, 852–857. https://doi.org/10.1038/s41587-019-0209-9.

STAR★METHODS

KEY RESOURCES TABLE

REAGENT or RESOURCE	SOURCE	IDENTIFIER
Antibodies		
Anti-UCP1 antibody	Abcam	Cat#ab10983; RRID: AB_2241462
SignalStain Boost IHC Detection Reagent (HRP, Rabbit)	Cell Signaling Techonologies	Cat#8114S; RRID: AB_10544930
Polyclonal Guinea Pig Anti-Insulin (Autostainer Link 48)	Agilent Dako	Cat#IR00261-2; RRID: AB_2800361
Chemicals, peptides, and recombinant proteins		
^{18}F-Fluorodeoxyglucose	Centre for Probe Development and Commercialization (CPDC)	imagingprobes.ca
Formalin	Sigma	Cat#HT501128
Paraffin	Sigma	Cat#1.07151
Xylene	Sigma	Cat#214736
Sodium citrate	Sigma	Cat#71498
PBS	Wisent	Cat#311-425-CL
SignalStain® DAB Substrate Kit	Cell Signaling Techonology	Cat#8059
Hematoxylin	Sigma	Cat#HHS16-500ML
Permount	FIsherChemical	Cat#SP15-500
TRIzol reagent	ThermoScientific	Cat#15596026
Chloroform	Sigma	Cat#288306
GeneJET RNA Purification Kit	ThermoScientific	Cat#K0731
Verso cDNA Synthesis Kit	ThermoFisher	Cat#AB1453B
PowerUp™ SYBR™ Green Master Mix	ThermoFisher	Cat#A25741
NucleoSpin Soil, Mini kit for DNA from soil	Macherey-Nagel	Cat#740780.50
KAPA2G Robust HotStart ReadyMix	Sigma	Cat#KK5701
Quant-iT™ PicoGreen™ dsDNA Assay Kit	ThermoScientific	Cat#P7589
Ampure XP beads	Beckman-Coulter	Cat#A63880
Critical commercial assays		
Insulin Mouse Serum Assay kit ^{HTRF}	Cisbio	Cat#62IN3PEF
Deposited data		
16S rRNA gene sequencing Fastq. files	This paper	BioProject accession number: PRJNA951705
Experimental models: Organisms/strains		
C57BL/6NTac	Taconic	Cat#B6NTac (GF)
Software and algorithms		
Qiime2	Qiime2 website	http://qiime2.org/
Qiime	Qiime website	http://qiime.org/
CellProfiler	Cellprofiler website	https://cellprofiler.org/
NDP.view2 Plus	Hamamatsu	Cat#U12388-01
Graphpad Prism 9	Graphpad website	https://www.graphpad.com/
R	CRAN	https://cran.r-project.org/
Rstudio	Posit	https://posit.co/
Metaboanalyst R	Xia Lab Github	https://github.com/xia-lab/MetaboAnalystR

CellPress
OPEN ACCESS

RESOURCE AVAILABILITY

Lead contact

Further information and requests for resources and reagents should be directed to the lead contact, Dana J Philpott (dana.philpott@utoronto.ca).

Materials availability

This study did not generate new unique reagents.

Data and code availability

- The 16S rRNA gene sequencing data were deposited into the Sequence Read Archive (SRA) of NCBI and can be accessed via BioProject accession number PRJNA951705. This information is also available in key resources table.
- This paper does not report original code.
- Any additional information required to reanalyse the data reported in this work paper is available from the lead contact upon request.

EXPERIMENTAL MODEL AND SUBJECT DETAILS

Human participants

The study was approved by the Research Ethics Board at the University Health Network (REB#15-8784). Patients were approached and consented to research after surgeons confirmed that the patients were suitable for bariatric surgery according to the criteria stated by the National Institutes of Health.[78] Inclusion criteria for this study included individuals $\geq$18 years and exclusion criteria included; previous gastrointestinal surgery that altered the anatomy, diagnosis of type 1 diabetes; regular intake of non-steroidal anti-inflammatory drugs; antibiotics, probiotics or prebiotics, or any experimental drug in the previous 3-month; smoking; pregnancy or breastfeeding. Clinical and biochemical data as well as fecal samples were collected at baseline (prior to the pre-surgical diet) and at 1- or 6-months post-RYGB. Patients' anthropometrics and medication history were taken by a registered nurse before RYGB and at 1 and 6-months post-RYGB. Plasma and serum were collected after a 12-hour fast and analyzed by the hospital's Laboratory Medicine Program using standardized methods. The homeostasis model for insulin resistance was also calculated using fasting insulin and glucose.[79] Fresh fecal samples were collected 12-hours before a scheduled appointment and stored in the participants' fridge.

Faecal sample collection

Patients were provided a kit to collect the stool sample at their house. This kit included a plastic collection/storage container with a lid, an insulated bag and cooling elements. Subjects were provided detailed instructions on how to collect, store and transport the sample. These samples were collected within 48 hours of each visit and stored in the patient's fridge. On the day of the appointment, patients transported the sample in the insulated bag with cooling agents. Once we received the sample it was processed, and the filtrates were kept in a -80°C freezer similar to previous studies.[80] This protocol was also used in other studies.[81,82]

Preparation of patient fecal samples

Following collection and upon receipt at clinic, stool samples were weighed out. Approximately 10g of feces were weighed in a Stomacher bag and combined with a sterile solution of 20% glycerol in saline. Samples were then homogenized by hand by squeezing the bags for approximately 1 min. The homogenates were then aliquoted into 1mL cryotubes and frozen for later use in FMT studies.

Mice and diet

We obtained GF mice from McMaster University's GF facility, which were housed and maintained accordingly in the University of Toronto GF facility. Mice were maintained in a pathogen-free, temperature-controlled, and 12 h light and dark cycle environment. All mice used in comparative studies were age-matched females. Human stool samples were collected at the following time points: 1) baseline prior to pre-bariatric surgery operation, 2) at the 1- or 6-months visits after surgery from 4 patients. Patient characteristics can be found in Table 1. The mice were fed with WD (Envigo, Cat #TD88137, 34% sucrose and 21% fat by weight) starting at 8-21 weeks of age, then gavaged with a single dose of pre- or post-RYGB human stool samples (200 μl of 1:5 diluted frozen fecal samples) in age and weight matched mice. Mice were then continually fed with WD for another 12 weeks before testing. Each mouse was singly caged throughout the experiment. All animal studies were approved by the Animal Care Committee at the University of Toronto.

METHOD DETAILS

In vivo metabolic studies

As previously described,[83] glucose tolerance tests (GTTs) were performed on mice fasted overnight, 14–16 h, using glucose 1.5 g/kg body weight injected intraperitoneally. Insulin tolerance tests were performed on mice fasted for 4 h, using insulin (Lilly) 1.5 U/kg body

weight. Measurements of blood glucose were taken at indicated time points after the injection. Serum insulin levels were measured by a HTRF insulin mouse serum assay kit (Cisbio, MA, USA).

Brown fat PET/CT scan

The details of this procedure are similar to the ones described by Wang et al.[84] The mice were fasted with free access to water and housed 14–16 h in a cold room at 4°C. Each mouse was removed from the cold room just prior to an intraperitoneal injection of 15 MBq ^{18}F-Fluorodeoxyglucose (^{18}FDG). Then the mouse was immediately anesthetized by inhalation with a mixture of 1.5–2% isoflurane and oxygen for 1 h to allow for FDG uptake.

At 1-h post-injection, a 10-min static image of the whole body was acquired on a Focus 220 microPET (Siemens Preclinical Solutions, Knoxville TN). Following PET imaging, each mouse was transferred, via a Minerve (Esternay, France) imaging bed, to a GE eXplore Locus Ultra microCT scanner (GE Healthcare, London ON). CT scans were acquired using routine parameters (80 kVp, 50 mA, voxel size of 154 μm × 154 μm × 154 μm) in order to obtain an anatomical reference. PET images were reconstructed with a maximum a posteriori reconstruction algorithm without attenuation correction onto a 256 × 256 matrix using a zoom of 6.5 (voxel size ~160 μm × 160 μm x 800 μm).

The PET and CT datasets were imported, co-registered and analyzed using Inveon Research Workplace 4.0 (IRW) software (Siemens Medical Solutions USA, Inc., Washington, DC). Volumes-of-interest were created around interscapular brown adipose tissue (BAT) and normal tissue/background. FDG uptake in BAT and normal tissue was expressed as percent injected dose per gram tissue (%ID/g) with decay correction. This animal study was under the Animal Use Protocol (2573.3) approved by the Animal Care Committee at the University Health Network.

Metabolic cage studies

As previously described,[85] mice were individually placed in automated metabolic cages with free access to food and water (Comprehensive Lab Animal Monitoring System-CLAMS from Columbus Instruments Company, Columbus, Ohio, USA) for 48 h. After 24-h acclimation to the apparatus, data for next 24 h were collected and analysed. Airflow was held at 0.5 L/min, food and water consumption were determined by weighing food or measuring water volume before and after 24- hour period. Metabolic activity was assessed using indirect calorimetry recording maximal O_2 consumption (VO_2), CO_2 production (VCO_2), and heat production normalized to body weight. The respiratory exchange ratio was calculated as VCO_2/VO_2. Energy expenditure was adjusted for body mass using ANCOVA.[86] Data are the average between light and dark measurements.

Haematoxylin and eosin (H&E) staining of BAT and VAT

BAT and VAT were collected and then fixed for 24–36 h in 10% (v/v) formalin and subsequently embedded in paraffin. Paraffin-embedded tissues were micro-sectioned at a thickness of 5 μm. The slides were stained with H&E using standard procedure. The images were acquired by using an Zeiss AxioObserver Z1 microscope.

Immunohistochemistry for BAT

Brown adipose tissues were harvested and fixed in 10% (v/v) formalin. The fixed tissues were embedded in paraffin and micro-sectioned at a thickness of 5 μm. The sections were then deparaffinized in xylene and rehydrated using an ethanol gradient. Heat-induced epitope retrieval was performed with citrate buffer (pH 6.0) at 95°C for 30 min. Upon cooling at room temperature for 20 min, slides were washed with PBS. Sections were then treated with blocking solution (3% goat serum in PBST) for 30 min at room temperature to block nonspecific binding. The slides were incubated with primary antibody UCP1 (Abcam- ab10983, 1:500) in PBST with 1% goat serum overnight at 4°C. The sections were washed the following day with PBS. The endogenous peroxidase activity was quenched with 0.3% hydrogen peroxide for 15 min at room temperature. After washing, slides were incubated with secondary HRP antibody (CST) against rabbit IgG at room temperature for 1 h. Slides were treated with a working solution of SignalStaina® DAB Substrate Kit (CST; Cat#8059). All sections were counterstained with hematoxylin and mounted with Permount (FisherChemical). Images were taken on a Zeiss AxioObserver Z1 microscope using the Zen software. Images were quantified using the CellProfiler cell image analysis software.

CellProfiler analysis of BAT

CellProfiler was used to quantify lipid droplet size and number. Images of H&E-stained tissue were converted to grayscale, uneven illumination was corrected, colours were reversed, noise was reduced by smoothing and suppressing grainy features, and images were thresholded for object identification. These objects were filtered with parameters of Compactness (maximum 1.8), Form Factor (minimum 0.5), Area (minimum 675), and Perimeter (maximum 1400) to exclude objects not corresponding to lipid droplets. Objects were overlaid on original images to confirm successful identification of lipid droplets. Measured area was converted to square micrometers (factor identified using scalebar and ImageJ).

CellProfiler was used to quantify relative UCP1 positive area. Images of brown adipose tissue were converted to grayscale and inverted before thresholding for recognition of lipid droplets (correction factor 1.6) and UCP1 positive area (correction factor 1.2). Objects were overlaid on original images to confirm successful identification of lipid droplets. The dimensions and area occupied by each were measured. Data are represented as UCP1 positive area relative to UCP1 area plus lipid droplet area in order to exclude background other inconsistent tissue features.

CellProfiler analysis of VAT

All image analyses were performed while blinded to sample groupings, and identical parameters were used to analyze each experimental group. CellProfiler was used to quantify adipocyte area. Slidescanner images were split into 1024x1024 pixel tiles. Images were converted to grayscale, uneven illumination was corrected, and noise was reduced before thresholding and recognizing objects. These objects were filtered with parameters of Area (2000-90,000 pixels), Form Factor (minimum 0.66), Minimum Feret Diameter (0.45), and Mean Radius (minimum 10) to exclude objects not corresponding to adipocytes. Objects were overlaid on original images to confirm successful identification of adipocytes. Adipocyte area was converted to square micrometers (factor identified using scalebar and ImageJ).

Islet morphometry

Pancreatic tissues from pre- and post-RYGB FMT mice were fixed for 24 hours in 4% paraformaldehyde in PBS (pH 7.4). Paraffin sections (7 μm thick) were obtained separately from pancreas and stained for insulin (Dako Canada) (catalog IR00261-2). Insulin-immunostained sections were scanned using an Olympus VS120 slide scanner and analyzed with NDP.view2 plus software from HAMAMATSU. Insulin immunostaining was calculated by an automated positive pixel count algorithm to determine total β-cell area, islet number per total pancreatic area, and islet size.[87]

Quantitative real-time PCR to analyze relative gene expression

Mouse subcutaneous and visceral adipose tissue stored at −80°C was used for the RNA isolation. RNA isolation from adipose tissue was performed using TRIzol™ Reagent (Life Technologies) as described by Cirera S[88] with some modifications. To isolate total RNA, approximately 100 mg of tissue was used. The homogenization was done in 1 mL of TRI Reagent using a bead beater homogenizer. After homogenization, the samples were incubated at room temperature for 5 min. Subsequently a centrifugation was done at 12000 g at 4°C for 10 min and the resulting fat monolayer was carefully avoided when pipetting the rest of the sample into a clean 1.5 mL tube. 200 μL of chloroform was then added to the sample and mixed by vortexing. After 3 min at room temperature the sample was centrifuged at 12000 g at 4°C for 10 min. After centrifugation, the upper phase was collected in a separate tube without disturbing the interphase. RNA was precipitated with 100% ethanol and the sample was then loaded on GeneJET RNA Purification Column (Thermo Scientific™). After this step the RNA was extracted as per the manufacturer's instructions. cDNA was synthesized using the Verso cDNA synthesis kit (ThermoFisher Scientific) according to manufacturer's instructions. cDNA was diluted accordingly, and Real-time PCR was performed in duplicate with PowerUp™SYBR™ Green Master Mix (ThermoFisher Scientific) and was run on a CFX384 Touch Real-Time PCR Detection System (Bio-Rad, Hercules, USA). The relative expression of genes was calculated with the formula $2^{-\Delta\Delta Ct}$. Murine *36b4* and *Tbp* was used as an endogenous control housekeeping gene. Primer sequences are listed in Primers used in RT-qPCR.

Primers used in RT-qPCR

Gene	Forward primer (5'-3')	Reverse primer (5'-3')
Tnf-α	AGCCCCCAGTCTGTATCCTT	CTCCCTTTGCAGAACTCAGG
Ccl2	CCTGCTGCTACTCATTCACCA	ATTCCTTCTTGGGGTCAGCA
Elane	CAGAGGCGTGGAGGTCATTT	CTACCTGCACTGACCGGAAA
Sirt1	GGTATCTATGCTCGCCTTGC	ACACAGAGACGGCTGGAACT
Il2ra	AACCACCACAGACTTCCCACAA	TTCCTCCATCTGTGTTGCCAG
sSt2	AAGGTCGAAATGAAAGTTCCAGC	GCCAATTTATTCAAGCAATGTGTG
St21	TGCATTTATGGGAGAGACCTGTTA	TGTGCAGAGCAATCTCCTGC
Il33	CCTCCCTGAGTACATACAATGACC	GTAGTAGCACCTGGTCTTGCTCTT
Adgre1	CTTTGGCTATGGGCTTCCAGTC	GCAAGGAGGACAGAGTTTATCGTG
Nos	GTTCTCAGCCCAACAATACAAGA	GTGGACGGGTCGATGTCAC
IL1b	GCAACTGTTCCTGAACTCAACT	ATCTTTTGGGGTCCGTCAACT
IL10	GCTCTTACTGACTGGCATGAG	CGCAGCTCTAGGAGCATGTG
Ucp1	ACTCAGGATTGGCCTCTACG	CCACACCTCCAGTCATTAAGC
Cox8b	GAACCATGAAGCCAACGACT	GCGAAGTTCACAGTGGTTCC
Pat2	GTGCCAAGAAGCTGCAGAG	TGTTGCCTTTGACCAGATGA
36b4	GCTCCAAGCAGATGCAGCA	CCGGATGTGAGGCAGCAG
Rpl19	GCATCCTCATGGAGCACAT	CTGGTCAGCCAGGAGCTT

16S rRNA gene amplicon sequencing

Total DNA was extracted from samples using the MoBio PowerSoil kit (MoBio) following manufacturer's instructions for increased yield. The V4 hypervariable region of the 16S rRNA gene was amplified using barcoded 515F (forward) and 806R (reverse) sequencing primers to allow for multiplexing.[89] Amplification reactions were performed using 12.5 uL of KAPA2G Robust HotStart ReadyMix (KAPA Biosystems), 1.5 uL of 10 uM forward and reverse primers, 7.5 uL of sterile water and 2 uL of DNA. The V4 region was amplified by cycling the reaction at 95°C for 3 min, 18x cycles of 95°C for 15 s, 50°C for 15 s and 72°C for 15 s, followed by a 5 min 72°C extension. All amplification reactions were done in triplicate to reduce amplification bias, pooled, and checked on a 1% agarose TBE gel. Pooled triplicates were quantified using PicoGreen and combined by even concentrations. The library was then purified using Ampure XP beads and loaded on to the Illumina MiSeq for sequencing according to manufacturer instructions (Illumina, San Diego, CA). Sequencing was performed using the V2 (150bp x 2) chemistry.

Quantitative real time PCR to analyze relative abundance of bacterial groups

Total DNA was extracted from the fecal pellet samples (mice and human patients) using the MoBio PowerSoil kit (MoBio, cat. 12888) following manufacturer's instructions. Bacterial DNA (~10 ng/μL) was analyzed by qPCR using 16S rRNA primers (Integrated DNA Technologies) to target specific groups (Quantitative real time PCR primers for bacterial group-specific16S rRNA), similar to our previous study.[90] These include *Akkermansia, Blautia*, Lachnospiraceae and Ruminococcaceae. Relative abundances of bacterial groups were calculated by normalizing ΔCt for each target group to the Eubacteria (housekeeping control) group.

Quantitative real time PCR primers for bacterial group-specific 16S rRNA

Bacterial Target Group	Forward primer (5'-3')	Reverse primer (5'-3')
Akkermansia muciniphila	CCTTGCGGTTGGCTTCAGAT	CAGCACGTGAAGGTGGGGAC
Blautia	CGGTACCTGACTAAGAAGC	GTTCCTCCTAATATCTACGC
Ruminococcaceae	GGCGGCYTRCTGGGCTTT	CCAGGTGGATWACTTATTGTGTTAA
Lachnospiraceae	AAACAGCTTAGTGGCGGACG	GGCTACTGATCGTCGCTTTG
Eubacteria 16S (F340-R514)	ACTCCTACGGGAGGCAGCAGT	ATTACCGCGGCTGCTGGC

Metabolite analysis

Metabolites were measured by The Metabolomic Innovation Centre (University of Alberta, AB, Canada). After extracting metabolites using 3-fold volume of 15 mL MeOH + 85 mL phosphate buffer (10 mM), metabolites were measured by combining direct injection mass spectrometry and a reverse-phase LC-MS/MS with some modifications.[91,92] Mass spectrometric analysis was performed on an ABSciex 4000 QTrap® tandem mass spectrometry instrument (Applied Biosystems/MDS Analytical Technologies, Foster City, CA) equipped with an Agilent 1260 series UHPLC system (Agilent Technologies, Palo Alto, CA).

QUANTIFICATION AND STATISTICAL ANALYSIS

Processing of 16S rRNA sequencing data: The UNOISE pipeline, available through USEARCH v11.0.667 and vsearch v2.10.4, was used for merging paired reads and quality filtering.[93–95] Assembled sequences were mapped back to the chimera-free denoised sequences at 99% identity OTUs. Taxonomy assignment was executed using SINTAX, available through USEARCH, and the UNOISE compatible Ribosomal Database Project (RDP) database version 16, with a minimum confidence cutoff of 0.8.[96] OTU sequences were aligned using align_seqs.py v.1.9.1 through QIIME1.[97]

Statistical analysis of 16S rRNA sequencing data: Estimates of alpha diversity and beta diversity (Bray-Curtis), PCoA plot generation, Procrustes analysis, and ANCOM[98] were performed in Qiime2.[99] Alpha diversity and relative abundances were calculated using datasets rarefied to the lowest number of reads per sample. PERMANOVA was used to test for differences in beta diversity between pre- and post-surgery groupings of humans and mice. The p-value was corrected by the Benjamini-Hochberg method. ANCOM was used to identify bacterial families or genera that significantly differed between groups. ANCOM accounts for the compositional nature of the relative abundance data and relies on the analysis of differences in pairwise log-ratios while controlling for false discoveries. We applied ANCOM with FDR correction of 0.05. A high "w score" generated by this test indicates the greater likelihood that the null hypothesis can be rejected, indicating the number of times a parameter is significantly different between groups.

Statistical analysis of targeted metabolite data: Targeted metabolomics analysis was performed using Metaboanalyst R plugin. Samples with over 50% missing values were omitted from analysis. Missing values were then replaced with values at 1/5 of the lowest detectable measurement for a given metabolite. Values were then log-transformed and scaled. Fold change analysis and unpaired

t-test were performed using cutoffs of FC>2 and p<0.05 respectively. PERMANOVA was used to determine broad differences between metabolites amongst pooled pre- and post- surgery groupings. PCA plots, volcano plots and heatmaps were also performed using Metaboanalyst and graphed using Graphpad Prism 9.

All graphs were prepared and statistical analysis performed using GraphPad Prism 9.0 (GraphPad Software). The statistical significance of the differences between various treatments or groups was measured by Permanova or Student's t test or Wilcoxon test. All the results are expressed as means ± S.E.M. P < .05 was considered statistically significant, *P < .05; **P < .005; ***P < .0005 and ****P <0.0001.